

# **Smearred Crack Approach: Back to the Original Track**

M. Cervera  
M. Chiumenti

# **Smearred Crack Approach: Back to the Original Track**

M. Cervera  
M. Chiumenti

**Publication CIMNE N<sup>o</sup>-295, November 2006**

# Smearred crack approach: back to the original track

M. Cervera and M. Chiumenti

International Center for Numerical Methods in Engineering (CIMNE)

Technical University of Catalonia (UPC)

Edificio C1, Campus Norte, Jordi Girona 1-3, 08034 Barcelona, Spain.

**KEYWORDS:** tensile cracking, strain softening, strain localization, damage, tracking algorithms, mesh dependence.

## Abstract

This paper reviews briefly the formulations used over the last 40 years for the solution of problems involving tensile cracking, both with the discrete and smeared crack approaches. The paper focuses in the smeared approach, identifying as its main drawbacks the observed mesh-size and mesh-bias spurious dependence when the method is applied “straightly”. A simple isotropic local damage constitutive model is considered, and the (exponential) softening modulus is regularized according to the material fracture energy and the element size. The continuum and discrete mechanical problems corresponding to both the weak discontinuity (smeared cracks) and strong discontinuity (discrete cracks) approaches are analyzed and the question of propagation of the strain localization band (crack) is identified as the main difficulty to be overcome in the numerical procedure. A tracking technique is used to ensure uniqueness of the solution, attaining the necessary stability and convergence properties of the corresponding discrete finite element formulation. Numerical examples show that the formulation derived is well posed, stable and remarkably robust. As a consequence, the results obtained do not suffer from spurious mesh-size or mesh-bias dependence, comparing very favorably with those obtained with other fracture and continuum mechanics approaches.

# 1 Introduction

Cracking is an essential feature of the behaviour of concrete structures. Even under service loads, concrete structures are normally full of cracks. They may be present as basic defects in the constituent materials, or they may be induced by inadequate design or construction or during service life. Clearly, tensile cracking must be taken into account in predicting ultimate load capacity as well as service behavior.

The tensile fracture of concrete is regarded as (quasi)brittle. Concrete has no yield behavior as exhibited by metals. Its tensile stress-strain diagram is nearly linear up to the peak stress, whereupon it immediately starts to descent. In spite of this, concrete shows considerable toughness. This toughness is related to the existing of a descending branch in the nominal stress-strain curve. This is known as strain softening.

Tensile cracking, with similar behavior to that of concrete, is also of primary concern in advanced composite materials, and in specific brittle materials like ceramics, glass and ice.

Therefore, it was very soon realized that means for assessing the stability of tensile cracks were necessary. The first one to wonder about the phenomenon of cracking was Galileo Galilei [1], in the XVII century. In 1921, A. A. Griffith [2], a British aeronautical engineer, introduced the first *fracture mechanics theory*, from observations done during his investigation on the fracture of glass sheets. For Griffith, a crack becomes unstable when the elastic energy stored by the material around the tip of the existing crack is greater than the energy necessary for extending the crack. In 1959 and 1960, Barenblatt [3] and Dugdale [4] introduced the concept of cohesive forces in the crack tip region, the first within the limits of elasticity theory and the second assuming an elastic-perfectly plastic material behaviour. These were the first attempts to bring closer the two different existing theories of Solid Mechanics: *fracture mechanics* (FM) and *continuum mechanics* (CM).

Also in the 1960's, digital computers and the Finite Element Model (FEM) started to be used by structural engineers in their attempts to obtain and quantify solutions in Structural and Solid Mechanics. With the evolving of time, this has eventually led to two different conceptions of the phenomenon of tensile cracking: the *discrete* and the *smearred crack approaches*.

Although nowadays many structural engineers and computational solid FE codes are decanted in favor of the smeared crack approach, the observed mesh-size and mesh-bias dependence make the academic world very suspi-

cious about the solutions obtained within this format. A lot of effort has been spent in the last 40 years to investigate and remedy the observed drawbacks of this approach.

It will be shown in this paper that the difficulties encountered in crack propagation problems when using the smeared crack approach are not related neither to the format of the standard continuum equations nor to the local definition of the constitutive laws considering softening. In recent papers ([5] and [6]) it is shown that mesh objective solutions, convergent upon refinement and exhibiting highly localized shear bands (or slip lines), can be obtained using local  $J_2$ -plasticity and damage models. The key to obtain these satisfactory solutions is to overcome the incompressibility constraint posed by the isochoric flow of inelastic strains imposed by the constitutive model. This is achieved by (i) using the suitable mixed format of the balance equations (which include the appropriate continuity equation) and (ii) using an stabilization technique especially designed to stabilize the selected interpolation fields for the primary variables (displacements and pressure). Hence, it must be concluded that with the appropriate (standard) continuum framework and with (standard) local constitutive models, the problem can be solved if the shortcomings of the spatial discretization used are satisfactorily surmounted.

As a consequence, the objectives of this paper are threefold: (i) to *investigate the numerical difficulty* that causes the mesh bias encountered in tensile localization problems when using the classical smeared crack approach, (ii) to *propose a numerical procedure* to overcome the identified numerical difficulty, and (iii) to *assess the performance* of the proposed procedure by means of solving selected numerical examples which exhibit tensile cracking.

The outline of the paper is as follows. In the next section we briefly review the main historical developments occurred both in the discrete and smeared crack approaches in the last 40 years, focusing in the several difficulties encountered along the way. Then, a simple isotropic scalar Rankine damage model, suitable for degradation under tensile straining, is presented. The necessary regularization of the softening modulus according to the size of the elements inside the localization band is discussed. Later, the corresponding standard irreducible boundary value problems for the so-called *weak and strong discontinuity approaches* are formulated. Strong and weak forms of the corresponding continuum and discrete problems are presented and the well posedness of the resulting equations is discussed. Also, the well known difficulties of solving localization problems using this standard, weak

discontinuity, local formulation are explained. Both mesh size and mesh bias dependence are discussed. Tracking of the crack through the fixed FE mesh is presented as a remedy to overcome this last difficulty. Also, a Section is include to discuss the theoretical and practical difficulties posed by the so-called non local constitutive models. Finally, selected numerical examples are presented to assess the present formulation and to show the attained benefits as compared to the “straight” use of the standard local formulation.

## **2 Discrete and smeared approaches to crack propagation**

### **2.1 Discrete crack approach**

The earliest applications of the FEM to concrete structures, back in the 1960’s, already dealt with the problem of crack propagation and they were some of the first nonlinear structural applications of the method ([7], [8], [9]). They focused on two essential ingredients: how to insert a crack in a FE mesh and the criteria for crack instability and direction of crack growth. Today, after more than four decades, these questions remain open to discussion in the research community.

In those early days, cracks were modelled by separation of nodal points initially occupying the same spatial position. An obvious restriction of such models is that cracks can only be formed along the element boundaries (Fig. 1a). Thus, the response is strongly mesh-dependent. Furthermore, when a crack propagates, the topology of the mesh is changed, and the updating procedures are time consuming. The DC approach was later refined so that new elements could be introduced whose boundaries were along the spreading crack (Fig. 1b). This obviously reduces the mesh dependency of the approach, but then remeshing techniques are required and the computing time increases.

Although the primitive studies have been based in a simple maximum tensile stress criterion to decide on the moment of crack propagation, it was very early recognized that the stress and strain fields that develop at the tip of the crack are singular and stress criteria were not reliable. Then, Computational Fracture Mechanics was born as the natural consequence of Fracture Mechanics theory. Criteria for crack propagation and, eventually, the prediction of the direction of propagation come directly from this theory,

which is, mostly, based on energy criteria. Also, it was noted that standard FE were not appropriate to capture these singular stress and strain fields [10]; consequently, special FE were developed (see reference [11]).

Alternatively, in the last decade, an effort has been made to tackle the discretization problem directly. Recently, Belytschko and coworkers ([12], [13], [14]) have introduced the so-called *extended finite element method* (X-FEM), which effectively overcomes most of the cited disadvantages of the DC approach. The X-FEM allows for crack propagation without remeshing, at the expense of tracking the advance of the crack through the FE mesh and progressively enriching the nodal degrees of freedom with new ones that represent both the *displacement jumps across the crack* and the developed *singular field at the tip* of the advancing crack (Fig. 1c, where the “enriched” nodes are marked).

Other of these efforts to model discrete cracks without the need of remeshing is the so-called *strong discontinuity approach* ([15], [16], [17], [18], [19],

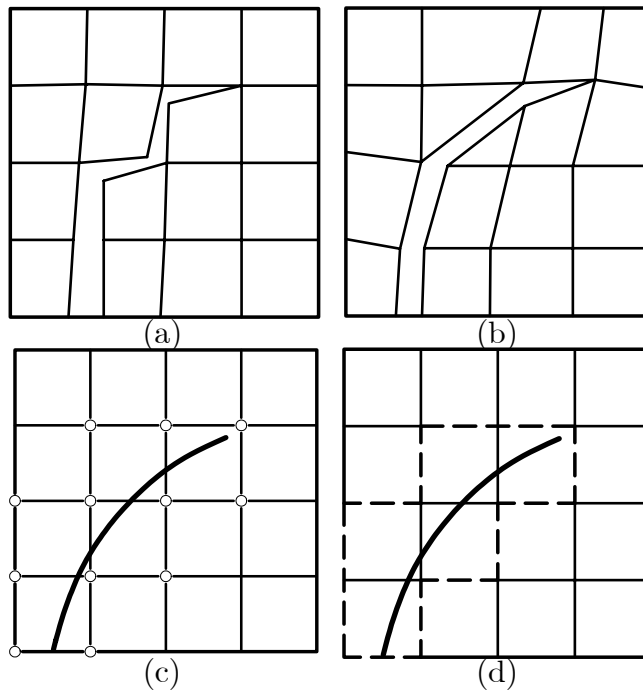


Figure 1: Discrete approaches to crack propagation: (a) without remeshing, (b) with remeshing, (c) with nodal enrichment and (d) with elemental enrichment

[20]). The strong discontinuity concept does not really depart from the usual Continuum Mechanics framework (as it will be shown below, its theoretical formulation is very similar to that of contact problems) but it leads to a new formulations for finite elements with “*embedded discontinuities*”, depending on the kinematical and statical assumptions adopted. Interestingly enough, their application invariably needs the use of “*tracking*” algorithms ([18], [20], [50], [21]), in order to establish which elements lie in the crack path and need to be enriched (Fig. 1d, where the elements with “embedded” discontinuities are marked). This, as the explicit control on the energy dissipated in the formation of the crack, represents another link with the well established tradition of fracture mechanics.

It is remarkable how the X-FEM, originated from Computational Fracture Mechanics has so many similarities with the Strong Discontinuity approach, originated from Computational Continuum Mechanics (see [19]).

## 2.2 Smearred crack approach

The smeared crack (SC) approach was born directly from Computational Continuum Mechanics. This means that, at least initially, the criteria for crack propagation and, eventually, the prediction of the direction of propagation came directly from this theory, which is, mostly, based on failure criteria expressed in terms of stresses or strains. SC models do not account for discontinuities in the topology of the FE mesh, so remeshing is unnecessary (Fig. 2a). On the contrary, the cracked material is assumed to remain

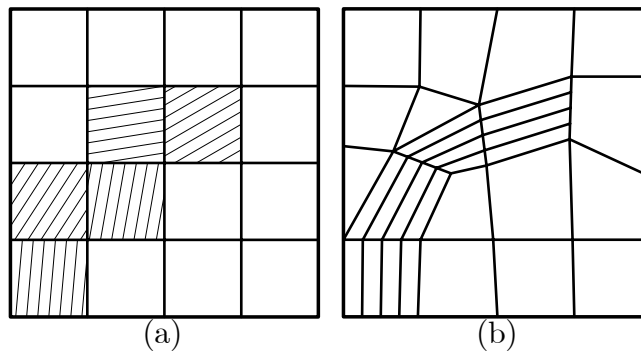


Figure 2: Smeared approaches to crack propagation: (a) without remeshing and (b) with remeshing



a continuum and the mechanical properties (stiffness and strength) are modified to account for the effect of cracking, according to the evolving states of strain and/or stress. This leads to the concept of generalized constitutive models, strongly nonlinear and with strain softening.

This approach was first used by Rashid in his 1968 historical paper [22] to study prestressed concrete pressure vessels. It must be said that the simplicity of this conception caught the attention of the engineering community immediately and, during many years, the smeared crack concept practically monopolized the field of crack propagation. The approach can be implemented in any nonlinear FE code by simply writing a routine for a new material constitutive model. Even today, more than 35 years later, most of the commercial FE codes use this approach, with little refinement over the original Rashid's ideas.

Unfortunately, it was very early realized in the 1970's that if a smeared crack is only one element across, the total energy dissipated in the cracking process is proportional to the size (the volume) of the element. Upon mesh refinement, for infinitesimally small elements, the dissipated energy vanishes. This is unacceptable from the physical point of view. The problem was satisfactorily solved in 1983, when Bazant and Oh [24] proposed the *crack band model*, which is essentially identical to the previous Hillerborg's [23] *cohesive crack model*, but developed in the context of CM and, therefore, easily implemented in standard FE codes. These new ideas showed that the always controversial concept of *strain softening* should not be considered as a characteristic of the material, but it is related to the *fracture energy* of the material and the *size of the FE* crossed by the smeared crack. This has certainly to be considered as a mile-stone in the road to crack modelization because it was the first serious success in bringing FM and CM theories to a common standpoint. Today, most of the commercial FE codes implement models with strain softening according to this idea of relating the dissipated energy to the fracture energy of the material.

In the 1980's, the constitutive models used were mostly orthotropic and max. principal stress driven. A lot of effort was devoted to the apparent "stress locking" effect that was observed when the directions of principal strain rotated along the analysis. Reference [25] presents a review of damage-based approaches for the fracture of quasi-brittle materials, linking them to the now old-fashioned, although still very popular, fixed and rotating smeared crack models of the 1980's.

Since the 1990's isotropic damage or plasticity models are usually pre-

ferred to model crack propagation. This choice implies that the macroscopic anisotropy of the structural behaviour has to be captured by means of the finite element approximation to within the resolution of the adopted mesh ([26], [27], [28], [29], [30]).

But once the problem of mesh-size dependence was quite satisfactorily overcome, a more difficult one was recognized. FE solutions based on SC suffer from mesh-bias dependence in such a strong manner that it can not be ignored. However, if the spatial discretization is designed in such way that an “appropriate” path for the advancing crack is available, the solutions obtained are immaculate (see Fig. 2b). In fact, remeshing has been suggested as a partial solution to this problem (see [31], [32]).

Since the early 1990’s until now, for more than a decade, a significant part of the research effort in Computational Solid Mechanics has been devoted to this problem. It is clear that in a *computational failure model*, set up within the CM framework, three pieces are necessary: (i) a continuum model that defines the variables and equations of the continuum BVP to be solved, (ii) a constitutive (material) model for the cracked and non-cracked parts of the domain, and (iii) a discretization procedure both in space and time that will turn the continuum differential equations into discrete algebraic equations. These three pieces are independent of each other; their basis must be established and their requirements must be fulfilled independently. If the resulting computational failure model has a flaw, its origin must be sought in one of the “pieces” of the puzzle. The well-known fact that “well-aligned” meshes produce good results strongly suggests that the flaw is in the spatial discretization procedure.

However, this evidence has not been generally recognized. Up to now, the disagreeable effects of mesh dependence have been attributed to the fact that, when strain-softening occurs and the slope of the local stress-strain curve becomes negative, the governing equations of the continuum problem lose their “natural” elliptic character. To remedy this, many so-called *non-local* constitutive models have been proposed in the last decade in different versions (*micropolar* models ([33], [34], [35]), *gradient-enhanced* models ([33], [37], [38], [39], [40], [41], [42], [43]), in different versions). All these strategies introduce a “localization limiter” (a length parameter) into the problem that effectively precludes the occurrence of sharp displacement gradients (strains).

After more than 35 years of research, it has come the moment of looking back to all the developments that have taken place, and to try to restore the original formulation of the smeared crack approach, that is, that crack prop-

agation can be solved efficiently within a local, rate-independent constitutive format.

Let us conclude this Section on the smeared crack approach with two remarks about isotropic continuum damage and strain softening:

- In the FM community a technique known as “element extinction” is sometimes used. This consists on simply deleting from the FE mesh those elements lying along the crack path. The results obtained are satisfactory if the finite element mesh used is fine enough. In a CM framework, the same can be done, but this “extinction” should be made with care, that is, taking into account the elastic energy released when performing it. This is, precisely, what an isotropic damage accomplishes: when the damage index reaches its final value,  $d = 1$ , the totally degraded element is effectively removed from the mesh; but this process takes place gradually, and while it is occurring the stored elastic energy is adequately released according to the brittleness of the particular element.
- It is often argued, particularly from the fracture mechanics community, that a material with negative tangential moduli is not a sound concept, as such material would be unstable and would not propagate waves. This is true, but the fact that the constitutive model, formulated in terms of *nominal* stresses and strains, contemplates strain softening does not mean that the real material softens. Damage models explicitly state that the stresses that the real material is sustaining are the *effective stresses*, which are not affected by damage; the lower *nominal stresses* are obtained by taking into account the *surface density of defects* in the damaged material, which is, by conception ([44], [45], [46]), the damage index. In this sense, the behaviour of the softening damaged material upon straining has perfect meaning as an average of the non-softening intact material and the growing density of defects that are developing inside it.

### 3 Isotropic Rankine damage model

#### 3.1 Constitutive model

The constitutive equation for the isotropic damage model is defined as:

$$\boldsymbol{\sigma} = (1 - d) \bar{\boldsymbol{\sigma}} = (1 - d) \mathbf{C} : \boldsymbol{\varepsilon} \quad (1)$$

where the effective stresses  $\bar{\boldsymbol{\sigma}}$ ,  $\bar{\boldsymbol{\sigma}} = \mathbf{C} : \boldsymbol{\varepsilon}$ , can be computed in terms of the total strain tensor  $\boldsymbol{\varepsilon}$ ,  $\boldsymbol{\varepsilon} = \nabla^s \mathbf{u}$ , where  $\mathbf{u}$  are the displacements,  $(\cdot)$  denotes the double contraction and  $d$ , the damage index, is an internal-like scalar variable whose definition and evolution is given below.

In the present work, the *equivalent stress* will assume the following form:

$$\tau = \langle \bar{\sigma}_1 \rangle \quad (2)$$

where  $\bar{\sigma}_1$  is the largest principal effective stress and  $\langle \cdot \rangle$  are the Macaulay brackets ( $\langle x \rangle = x$ , if  $x \geq 0$ ,  $\langle x \rangle = 0$ , if  $x < 0$ ).

With this definition for the equivalent effective stress, the damage criterion,  $\Phi$ , is introduced as:

$$\Phi(\tau, r) = \tau - r \leq 0 \quad (3)$$

where  $r$  is an internal stress-like variable that is interpreted as the current damage threshold, in the sense that its value controls the size of the (monotonically) expanding damage surface. The initial value of the damage threshold is  $r_o = \sigma_o$ , where  $\sigma_o$  is the initial uniaxial damage stress.

The expansion of the damage bounding surface for loading, unloading and reloading conditions is controlled by the Kuhn-Tucker relations and the damage consistency condition, which are

$$\dot{r} \geq 0 \quad \Phi(\tau, r) \leq 0 \quad \dot{r} \Phi(\tau, r) = 0 \quad (4a)$$

$$\text{if } \Phi(\tau, r) = 0 \text{ then } \dot{r} \dot{\Phi}(\tau, r) = 0 \quad (4b)$$

leading, in view of Eq. (3), to the loading condition

$$\dot{r} = \dot{\tau} \quad (5)$$

This, in turn, leads to the explicit definition of the current values of the internal variable  $r$  in the form

$$r = \max \{ r_o, \max(\tau) \} \quad (6)$$

Finally, the damage index  $d = d(r)$  is explicitly defined in terms of the corresponding current value of the damage threshold, so that it is a monotonically increasing function such that  $0 \leq d \leq 1$ . In this work, we will use the following exponential function:

$$d(r) = 1 - \frac{r_o}{r} \exp \left\{ -2H_S \left( \frac{r - r_o}{r_o} \right) \right\} \quad r_o \leq r \quad (7)$$

where  $H_S \geq 0$  is a constant.

### 3.2 Strain-softening and fracture width regularization

In FE analysis, the straight use of strain softening constitutive models entails the loss of objectivity of the results, in the sense that the strains tend to localize in a band that is only one element across, independently of the element size  $h_e$ . Upon mesh refinement, as  $h_e$  tends to zero, strains tend to concentrate on a band of zero thickness (a geometrical line), and no energy is dissipated in the failure process. Clearly, this is physically unacceptable.

In order to remedy this well-accounted for fact, Bazant and Oh [24] proposed the use of the so-called “*fracture energy regularization technique*”, nowadays used in many FE applications. This strategy is extremely convenient from the computational standpoint, while guaranteeing a correct dissipated energy upon mesh refinement.

The fracture energy regularization technique is based on the assumption that dissipation takes place in a band only one element thick, irrespective of the element size. The basic concept consists on modifying the softening law in such a way that the energy dissipated over a completely degraded finite element be equal to a given value, which depends on the fracture energy of the material and on the element size. In each element, the computational width of the fracture zone is called the *element characteristic length*  $l_{\text{ch}}$  [47].

The specific dissipated energy  $\mathcal{D}$  is then scaled for each element so that the equation

$$\mathcal{D} l_{\text{ch}} = \mathcal{G}_f \quad (8)$$

holds, where  $\mathcal{G}_f$  is the mode I fracture energy of the material, regarded to be a material property. This makes the softening modulus  $H_S$  dependent on the element size.

For the isotropic damage model with exponential softening it can be proved that the specific dissipated energy is

$$\mathcal{D} = \left(1 + \frac{1}{H_S}\right) \frac{\sigma_o^2}{2E} \quad (9)$$

and, therefore

$$H_S = \frac{\overline{H}_S l_{\text{ch}}}{1 - \overline{H}_S l_{\text{ch}}} \geq 0 \quad (10)$$

where  $\overline{H}_S = \sigma_o^2 / (2E\mathcal{G}_f)$  depends only on the material properties, as  $\mathcal{G}_f$  is the mode I fracture energy per unit area,  $\sigma_o$  is the uniaxial strength and  $E$  is the Young's modulus. Note that the *specific softening parameter*  $\overline{H}_S$  measures the brittleness of the material, while the *elemental softening parameter*  $H_S$  measures the brittleness of the finite element. It is clear from Eq. (10) that the introduction of the characteristic length implies a limitation on the maximum size of the finite elements used in the mesh,  $h_e \leq 1/\overline{H}_S$ . The greater the elements, the steeper is the softening branch of the response, and, locally, the fracture process is more brittle. For  $h_e > 1/\overline{H}_S$  the dissipated energy  $\mathcal{D} = \mathcal{G}_f/h_e$  is smaller than the elastic energy stored by the element, and a dynamic snap-back would occur at the onset of damage.

For linear simplicial elements, the characteristic length can be taken as the representative size of the element,  $l_{\text{ch}} = h_e$ . Assuming that the elements are equilateral, the size of the element can be computed as  $h_e^2 = (4/\sqrt{3}) A_e$  for triangular elements,  $A_e$  being the area of the element, and as  $h_e^3 = (12/\sqrt{2}) V_e$  for tetrahedral elements, where  $V_e$  is the volume of the element.

It is remarkable how this simple technique solves the problem of mesh-size dependence satisfactorily. To show this, consider the 1D problem of a straight bar under tensile straining, with a small defect located at a given position inside the bar. Obviously, the only reasonable solution is a crack initiating and progressively opening at the location of the defect. If the problem is solved with small enough time increments so to ensure that only the finite element containing the defect opens at the proper time step, and the element size is adequately taken into account to regularize the local softening, the global response of the bar, in terms of load vs. end displacement is unique and perfectly objective upon mesh refinement.

## 4 Boundary value problem

The possibilities to model tensile cracks with finite elements within the Continuum Mechanics framework are several, and both the weak and the strong discontinuity approaches have been followed. In the first, the objective is to capture the crack as precisely as possible, with standard continuous elements. In the second, the displacement field is enhanced with discontinuous functions so that the “true” discontinuity line can be captured. In fact, both approaches are perfectly compatible. On one hand, a weak discontinuity can be interpreted as the regularization of a strong one over a given width, for instance with the discontinuity “smeared” across the maximum possible resolution of the mesh, that is, one element; on the other hand, a strong discontinuity is the limit case of a weak one with vanishing width. Figure 3a sketches both approaches to strain localization.

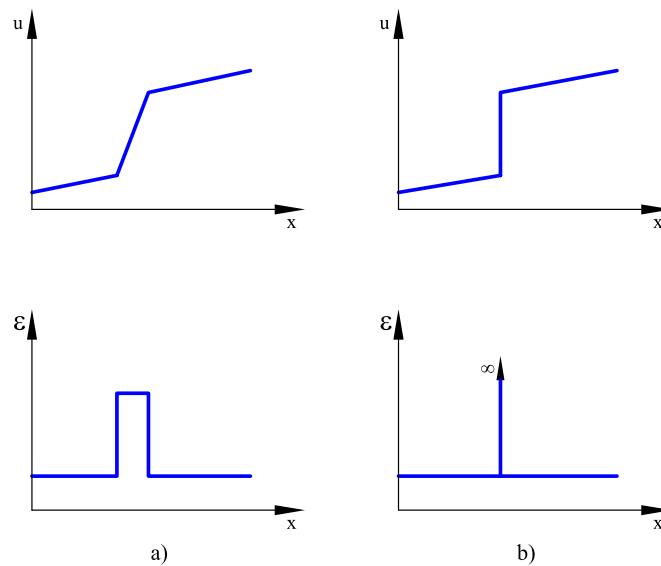


Figure 3: Strain localization: (a) weak discontinuity; (b) strong discontinuity

## 4.1 Weak and strong discontinuity approaches

### 4.1.1 Weak discontinuity approach

The strong form of the continuum mechanical problem can be stated as: find the displacement field  $\mathbf{u}$ , for given prescribed body forces  $\mathbf{f}$ , such that:

$$\nabla \cdot \boldsymbol{\sigma} + \mathbf{f} = \mathbf{0} \quad \text{in } \Omega \quad (11)$$

where  $\Omega$  is the open and bounded domain of  $\mathbb{R}^{n_{\text{dim}}}$  occupied by the solid in a space of  $n_{\text{dim}}$  dimensions. Eq. (11) is subjected to appropriate Dirichlet and Neumann boundary conditions. In the following, we will assume these in the form of prescribed displacements  $\mathbf{u} = \bar{\mathbf{u}}$  on  $\partial\Omega_u$ , and prescribed tractions  $\bar{\mathbf{t}}$  on  $\partial\Omega_t$ , respectively.

Note that in the following, the damage distribution is assumed to be known. The standard formulation merely states the problem for a given damage configuration; observe that, by itself, it does not include any criterion to trigger strain localization under increasing straining.

Multiplying by the test functions and integrating by parts, the associated weak form of the problem can be stated in the standard form as:

$$(\nabla^s \mathbf{v}, \boldsymbol{\sigma}) - (\mathbf{v}, \mathbf{f}) - (\mathbf{v}, \bar{\mathbf{t}})_{\partial\Omega_t} = 0 \quad \forall \mathbf{v} \quad \text{in } \Omega \quad (12)$$

where  $\mathbf{v} \in \mathcal{V}$  are the variations of the displacement field,  $\mathcal{V} = H^1(\Omega)$  is the space of continuous functions with discontinuous derivatives, and  $(\cdot, \cdot)$  denotes the inner product in  $L^2(\Omega)$ , the space of square integrable functions in  $\Omega$ .

The corresponding discrete problem is

$$(\nabla^s \mathbf{v}_h, \boldsymbol{\sigma}_h) - (\mathbf{v}_h, \mathbf{f}) - (\mathbf{v}_h, \bar{\mathbf{t}})_{\partial\Omega_t} = 0 \quad \forall \mathbf{v}_h \quad \text{in } \Omega \quad (13)$$

where  $\mathbf{v}_h$  and  $\boldsymbol{\sigma}_h$  represent the discrete counterparts of the fields  $\mathbf{v}$  and  $\boldsymbol{\sigma}$ .

In the *weak discontinuity approach*, the discrete displacement space  $\mathbf{u}_h$  consists of polynomial functions inside the elements and interelement continuity is enforced by nodal compatibility; therefore,  $\mathbf{u}_h$  is piece-wise continuous. The discrete stress field  $\boldsymbol{\sigma}_h$  is a continuous function (through the constitutive equation) of the discrete strain field,  $\boldsymbol{\varepsilon}_h = \nabla^s \mathbf{u}_h$ , which consists of polynomial functions (of one degree less than the displacements) inside the elements, but is discontinuous at the interfaces between elements. Therefore, strain localization can be *optimally* reproduced by highly localized displacement gradients (strains) across *one single element*.



### 4.1.2 Strong discontinuity approach

In the strong discontinuity approach ([15], [16], [17], [18], [19]) it is assumed that it exists a material discontinuity  $S \subset \Omega$  of zero measure (that is,  $S$  can be mapped onto  $\mathbb{R}^{(n_{\text{dim}}-1)}$ ) and that discontinuities in the displacement field may occur across  $S$  (see Fig. 4). This is the case of a line crack in 2D or a surface crack in 3D.

Note that in the following, the position and extension of the discontinuity  $S$  is assumed to be known. The formulation merely states the problem for a given configuration; it is emphasized that, by itself, it does not include any criterion to establish the stability of the crack or to govern its possible extension with time under increasing loading. This has to be derived from different considerations, like bifurcation analysis [17].

The strong form of the continuum mechanical problem can be stated as: find the (discontinuous) displacement field  $\mathbf{u}$ , for given prescribed body forces  $\mathbf{f}$ , such that:

$$\nabla \cdot \boldsymbol{\sigma} + \mathbf{f} = \mathbf{0} \quad \text{in } \Omega \setminus S \quad (14a)$$

$$\mathbf{t}^{\Omega \setminus S} = \mathbf{t}^S \quad \text{in } S \quad (14b)$$

where  $\Omega \setminus S$  is the part of  $\Omega$  outside the discontinuity  $S$ . Eq. (14a) is subjected to appropriate Dirichlet and Neumann boundary conditions. Note that Eq. (14a) represents internal equilibrium in each one of the two parts,  $\Omega^-$  and  $\Omega^+$ , in which  $S$  divides  $\Omega$ ; on the other hand, Eq. (14b) represents continuity

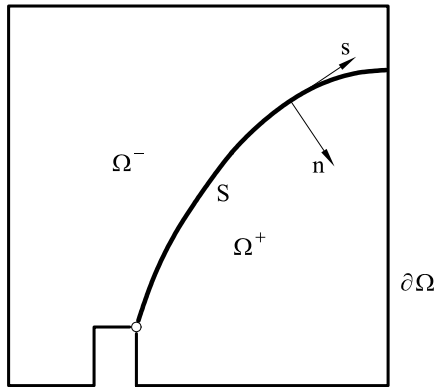


Figure 4: Strong discontinuity approach

of tractions across the discontinuity  $S$ . It can be observed that these are the same equations that govern *contact* between two bodies.

Multiplying by the corresponding test functions and integrating by parts the first equation, the associated weak form of the problem can be stated in the form:

$$(\nabla^s \mathbf{v}, \boldsymbol{\sigma}) - (\mathbf{v}, \mathbf{f}) - (\mathbf{v}, \bar{\mathbf{t}})_{\partial\Omega_t} = 0 \quad \forall \mathbf{v} \quad \text{in } \Omega \setminus S \quad (15a)$$

$$(\tilde{\mathbf{v}}, \mathbf{t}^{\Omega \setminus S}) - (\tilde{\mathbf{v}}, \mathbf{t}^S) = 0 \quad \forall \tilde{\mathbf{v}} \quad \text{in } S \quad (15b)$$

where  $\mathbf{v} \in \mathcal{V}$  are the variations of the continuous part of the displacement field,  $\mathcal{V} = H^1(\Omega)$ , and  $\tilde{\mathbf{v}} \in \tilde{\mathcal{V}}$  are the variations of the discontinuous part of the displacement field,  $\tilde{\mathcal{V}} = L^2(\Omega)$ . Note that the displacement field  $\mathbf{u}$  in  $\Omega$  is discontinuous across  $S$  and it can be split as  $\mathbf{u} = \bar{\mathbf{u}} + \tilde{\mathbf{u}}$ , where  $\bar{\mathbf{u}}$  is continuous in  $\Omega$  and  $\tilde{\mathbf{u}}$  is discontinuous across  $S$ . Eq. (15b) is necessary to determine  $\tilde{\mathbf{u}}$ .

Note that the stress field  $\boldsymbol{\sigma}$  needs to be defined only in  $\Omega \setminus S$ , and not at  $S$ . In fact, to solve the problem it is necessary to relate the *tractions*  $\mathbf{t}$  to the displacement *jumps* across  $S$ . This would call for a *decohesive traction versus jump* law at the interface, and there would be no necessity of introducing the concept of a *softening stress versus strain* law for the material in the solid domain. However, the following artifice is possible. Let us extend the definition of the stress field  $\boldsymbol{\sigma}$  in  $S$  in such a way that

$$\mathbf{t}^S = \boldsymbol{\sigma}^S \cdot \mathbf{n} \quad \text{in } S \quad (16)$$

where  $\mathbf{n}$  is a unit vector orthogonal to  $S$  (see Fig. 4). In this way, the decohesion law relating tractions with displacement jumps can be interpreted as the projection onto  $S$  of a strain-softening constitutive law relating (certain components of the) stress with (certain components of the) strain, defining the strain tensor in  $S$  as  $\boldsymbol{\varepsilon} = \nabla^s \mathbf{u}$ , in a distributional sense ([17], [48]).

The corresponding discrete problem is

$$(\nabla^s \mathbf{v}_h, \boldsymbol{\sigma}_h) - (\mathbf{v}_h, \mathbf{f}) - (\mathbf{v}_h, \bar{\mathbf{t}})_{\partial\Omega_t} = 0 \quad \forall \mathbf{v}_h \quad \text{in } \Omega \setminus S \quad (17a)$$

$$(\tilde{\mathbf{v}}_h, \mathbf{t}_h^{\Omega \setminus S}) - (\tilde{\mathbf{v}}_h, \mathbf{t}_h^S) = 0 \quad \forall \tilde{\mathbf{v}}_h \quad \text{in } S \quad (17b)$$

where  $\mathbf{v}_h, \tilde{\mathbf{v}}_h$  and  $\boldsymbol{\sigma}_h, \mathbf{t}_h$  represent the discrete counterparts of the fields  $\mathbf{v}, \tilde{\mathbf{v}}$  and  $\boldsymbol{\sigma}, \mathbf{t}$ .

In the *strong discontinuity approach*, several possibilities appear when defining the spatial discretization of the displacement field. One of them

is to use finite elements with *embedded discontinuities*. Here, the elements crossed by the discontinuity, *and only them*, are enriched with additional degrees of freedom to parametrize the discontinuous part  $\tilde{\mathbf{u}}$ . Precisely, Eq. (17b) is necessary to determine these additional dofs. Therefore, the discrete displacement space  $\mathbf{u}_h$  is piece-wise continuous in  $\Omega \setminus S$ , but discontinuous across  $S$ . The discrete strain field  $\boldsymbol{\varepsilon}_h$  consists of polynomial functions (of one degree less than the displacements) inside the elements and discontinuous at the interfaces between elements in  $\Omega \setminus S$ , but grows to infinity across  $S$ . Figure 3b shows this situation.

## 4.2 Well posedness, ellipticity and stability

Over the last years, many researchers have supported the idea that the underlying reason why the standard, local, rate-independent constitutive models are inadequate to model localized straining correctly is the local change of character of the governing equations (see, for instance, [33], [34], [35], [36], [37], [38], [39], [40], [41], [42], [43]). Let us consider this question by considering both the weak and strong discontinuity approaches.

The governing Eq. (11) can be rewritten in term of the deviatoric and volumetric parts of the deformation as

$$\nabla \cdot (G \nabla^s \mathbf{u}) + \nabla (K \nabla \cdot \mathbf{u}) + \mathbf{f} = \mathbf{0} \quad \text{in } \Omega \quad (18)$$

where  $G$  and  $K$  are the shear and bulk moduli, respectively.

A standard stability (or energy) estimate for problem (18) is obtained by multiplying the left hand side by  $\mathbf{u}$  and integrating by parts over the domain  $\Omega$ , to yield

$$(\nabla^s \mathbf{u}, G \nabla^s \mathbf{u}) + (\nabla \cdot \mathbf{u}, K \nabla \cdot \mathbf{u}) = \|\mathbf{u}\|_E^2 > 0 \quad (19)$$

where  $\|\cdot\|_E^2$  is the energy norm (equal to the elastic free energy). For strictly positive elastic moduli,  $G, K > 0$ , the elliptic character of the elastic governing equation is evident.

For an isotropic damage model, the governing equation reads

$$(\nabla^s \mathbf{u}, G_{\text{sec}} \nabla^s \mathbf{u}) + (\nabla \cdot \mathbf{u}, K_{\text{sec}} \nabla \cdot \mathbf{u}) = \|\mathbf{u}\|_E^2 > 0 \quad (20)$$

where the elliptic character of the equation can be guaranteed as long as the *secant* moduli,  $G_{\text{sec}} = (1-d)G$  and  $K_{\text{sec}} = (1-d)K$ , remain strictly positive, that is, for damage index  $d < 1$ . Eq. (20) still holds if the secant moduli

vanish completely ( $d = 0$ ) only in a subdomain  $S \subset \Omega$  of zero measure. The problem is obviously unstable if there are subdomains of non-zero measure in  $\Omega$  which lose the stiffness completely.

Regarding the discrete problem, the same restrictions apply for the governing equation

$$(\nabla^s \mathbf{u}_h, G_{\text{sec}} \nabla^s \mathbf{u}_h) + (\nabla \cdot \mathbf{u}_h, K_{\text{sec}} \nabla \cdot \mathbf{u}_h) = \|\mathbf{u}_h\|_E^2 > 0 \quad (21)$$

where  $\mathbf{u}_h$  represent the discrete displacement field. It would seem that ellipticity can only be maintained if  $\mathbf{u}_h$  is discontinuous (strong discontinuity), ensuring that the secant moduli vanish completely only in a subdomain of zero measure in  $\Omega$ . However, in a less strict sense, it can be stated that the problem remains elliptic if the secant moduli vanish only in a “properly restricted” subdomain in  $\Omega$ . This leaves the possibility of solving crack propagation problems using standard elements with continuous displacement fields  $\mathbf{u}_h$  (weak discontinuity) open, if the extension of the totally damaged areas is “properly restricted”. Also, the problem formulated in this way remains elliptic upon mesh refinement along the crack path.

## 5 The problem of crack propagation

### 5.1 Local approximation error

In Fracture Mechanics, the two basic ingredients of the physical model are: (a) the criterion for crack *propagation* (instability), which is usually established in terms of the stored elastic energy, and (b) the criterion for selecting the *direction* of crack propagation, which is established empirically among several possibilities [49]. Once these two ingredients are established, the problem of crack propagation is invariably tackled in a staggered, two stage, procedure: for a *given crack configuration*, (i) solve the mechanical problem in order to compute the stress field and, consequently, to determine if the crack is unstable and (ii) update the crack path, by advancing the crack tip a small distance, according to the selected criterion for crack propagation. No surprisingly, crack tracking algorithms are always an essential part of FM based codes, and are also crucial in the application of the X-FEM.

In a Continuum Mechanics framework, the same procedure can be followed, now involving: for a *given damage distribution*, (i) solve the mechanical problem in order to compute the stress field Eq. (21) and, consequently,

(ii) update the damage distribution. This second stage involves two different operations: (ii.a) to update the damage index in those elements previously damaged and (ii.b) to decide which elements are newly damaged.

Observe now the implications of proceeding in this way. Stage (i) consists of solving a *linear elastic* BVP, with a *given distribution of (positive) elastic moduli*. The problem is obviously *linear, well posed, elliptic, stable* and the solution is *unique*. Note also that while solving this problem it is never necessary to evaluate any negative *tangent* elastic modulus. Stage (ii.a) is trivial, as damage is an explicit function of the strain history. Stage (ii.b), deciding which elements are newly damaged, requires some more deliberation.

In the classical smeared crack approach it has always been implicitly understood that the criterion for the onset of cracking, which is always established in terms of stresses/strains, also must *automatically* define the direction of propagation. This is a natural assumption in the continuum problem, with proper evaluation of stress and strain values and directions. However, in the discrete problem the stress and strain fields evaluated in the vicinity of the crack tip differ greatly from being exact. In fact, the tip of the crack is a (nearly) singular point, and the  $L_\infty$ -norm of the error on the displacement gradients (strains) in the computed discrete solution is unbounded. As a consequence, the automatic application of the cracking criterion for the evaluation of the direction of crack growth leads to an unacceptable dependence on the mesh bias in this region.

*This local approximation error due to the spatial discretization in the vicinity of the crack tip is the only real difficulty to be overcome when solving the problem of tensile crack propagation.* When using the Fracture Mechanics approach, this was traditionally accomplished by the use of special finite elements in the discretization of this region (see reference [11]). More recently, the X-FEM applied to LEFM problems proves effectively that mesh bias is eliminated if the functional space of the discrete displacement field is enriched with functions that contain the *analytical solution* in the vicinity of the crack tip ([12], [13], [14]).

The same situation arises when using the Continuum Mechanics approach. Remarkably, and although it was not always explicitly stated, all successful applications of the strong discontinuity approach use tracking algorithms to lead the direction of crack propagation. In fact, Mosler and Meschke [50] have proved that if tracking is not used, the strong discontinuity formulation leads to the same spurious mesh bias dependence as the standard weak discontinuity approach.

All these evidences lead to the conclusion that solving in an adequate manner the problem of crack propagation (crack tracking) is essential also in a continuum framework of the crack growth problem, *both* if continuous or discontinuous displacement fields are used in the interpolation basis.

## 5.2 Evaluation of the propagation direction

In this work we will explicitly consider the evaluation of the propagation direction as a separate problem, obviously coupled to that of solving the internal equilibrium equation (13). This evaluation must be *consistently linked* to the cracking criterion, as this is the established cracking mechanism at continuum level, and it cannot be *locally dependent* on the discrete stress/strain fields, as these may be substantially off-track.

An essentially identical procedure was proposed in reference [18] in the strong discontinuity framework, and it has been already applied in 2D and 3D applications [20].

For a Rankine damage criterion, let us assume that the crack propagates following a surface (a line in 2D) which is orthogonal to the direction of the maximum positive principal stress. Let  $\mathbf{n}$  be a field of unit vectors in this direction at each point of the domain and  $\mathbf{s}$  and  $\mathbf{t}$  be any two orthogonal unit vectors orthogonal to it. Let  $\theta$  be a scalar field such that its gradient is parallel to the given vector field  $\mathbf{n}$ , so that  $\mathbf{n} = \nabla\theta / \|\nabla\theta\|$ . It is clear that the iso-level surfaces (lines in 2D) defined by  $\theta = cte$  are orthogonal to  $\mathbf{n}$ . Therefore, the crack propagates along one particular iso-level surface  $S$  defined by  $\theta = \bar{\theta}_o$ . Thus, the problem of evaluating the direction of crack propagation is equivalent to finding the scalar field  $\theta$  and determining the iso-level locus  $\theta = \bar{\theta}_o$ .

This is conveniently formulated as the following *evolutionary linear BVP*: find the scalar field  $\theta$ , such that:

$$C\dot{\theta} + \nabla \cdot (\mathbf{K} \cdot \nabla\theta) = \mathbf{0} \quad \text{in } \Omega \quad (22)$$

where  $\Omega$  is the open and bounded domain of  $\mathbb{R}^{n_{\text{dim}}}$  occupied by the solid in a space of  $n_{\text{dim}}$  dimensions.

Eq. (22) is subjected to appropriate initial and boundary conditions. In the following, we will assume that the initial conditions  $\theta(\mathbf{x}, t = 0) = \theta_o$  are selected to satisfy that  $\theta(\mathbf{x}_o, t = 0) = \bar{\theta}_o$  at the point(s)  $\mathbf{x}_o$  of the boundary where the crack is to be initiated; natural boundary conditions are imposed at

$\partial\Omega$ , except at (at least) two points selected as to ensure that  $\dot{\theta}(\mathbf{x}_o, t \geq 0) = 0$  (see Fig. 5a).

The coefficient  $C$  and the second-order tensor  $\mathbf{K}$  couple the scalar problem to the evolution of the mechanical solution, Eq. (11). Noting by  $\bar{S} \subset S$  the part of the iso-level surface  $S$  where the cracking criterion has already been violated (consolidated part of the crack), they take the following values:

$$C = \begin{cases} 0 & \text{if } \mathbf{x} \notin \bar{S} \\ 1/\varepsilon & \text{if } \mathbf{x} \in \bar{S} \end{cases}, \quad \mathbf{K} = \mathbf{s} \otimes \mathbf{s} + \mathbf{t} \otimes \mathbf{t} + \varepsilon \mathbf{n} \otimes \mathbf{n} \quad (23)$$

where  $\varepsilon$  is a small perturbation value. These values are defined to ensure that  $\dot{\theta} = 0$  for points  $\mathbf{x} \in \bar{S}$  of the already formed crack and that  $\mathbf{n} = \nabla\theta / \|\nabla\theta\|$ .

The associated weak form of the problem can be stated as:

$$\left( C\dot{\theta}, \eta \right) + (\mathbf{K} \cdot \nabla\theta, \nabla\eta) = 0 \quad \forall \eta \quad (24)$$

where  $\eta \in \mathcal{Q}$  are the variations of the scalar field,  $\mathcal{Q} = H^1(\Omega)$ . The corresponding discrete problem is

$$\left( C\dot{\theta}_h, \eta_h \right) + (\mathbf{K} \cdot \nabla\theta_h, \nabla\eta_h) = 0 \quad \forall \eta_h \quad (25)$$

where  $\theta_h$  and  $\eta_h$  are the discrete counterpart spaces of  $\theta$  and  $\eta$ . In the discrete problem, when the smeared crack approach is adopted, the ‘‘points’’ belonging to  $S$  must be understood as the elements crossed by the iso-surface (or line)  $S$ .

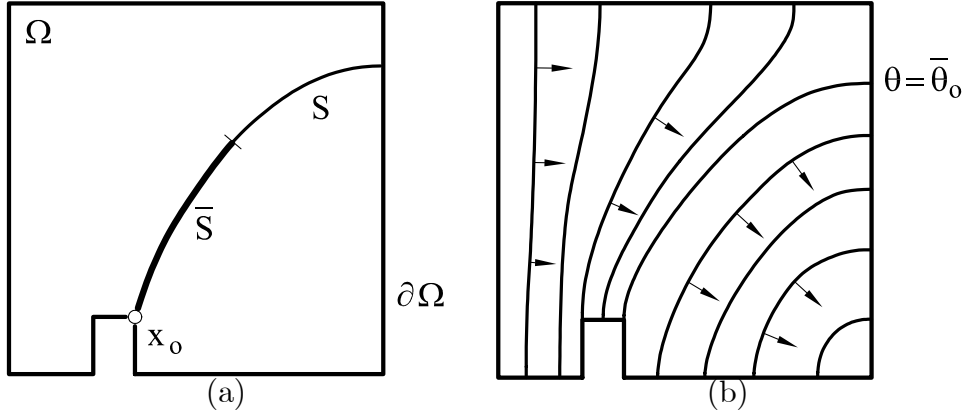


Figure 5: Tracking algorithm: (a) definition, (b) iso-level curves

Problem (25) is very simple, as it is linear, elliptic and it only involves one unknown per node. Besides, it is sufficiently well behaved (if  $\varepsilon = 0$ ,  $\mathbf{K}$  is singular) and it does not present any (nearly) singular point in the vicinity of the advancing crack. It can be solved in the same FE mesh as the mechanical problem and the coupling to it can be solved in a staggered manner once per time increment. Once it is solved, and the elements  $e$  lying along the iso-level curve  $S$ , such that  $\theta = \bar{\theta}_o$ , are identified, these are subsequently known to the mechanical solver when performing the check on the crack criterion; only those elements crossed by  $S$  are allowed to crack, and those actually cracked are added to the consolidated part of the track  $\bar{S} \subset S$ .

Implementation of equation (25) is straightforward in a standard FE framework [51], and it becomes trivial in those FE codes intended for coupled multifield formulations, such as thermo-mechanical or seepage-mechanical problems.

## 6 On nonlocality and strain localization

Since their advent in 1990 [46], precisely with an isotropic scalar damage model, the whimsical concept of nonlocal constitutive models, applied to strain localization problems, has become very popular and been the subject of innumerable publications. A recent and extensive review of their development can be found in [43].

Regardless of their trendiness, nonlocal models pose several theoretical and practical difficulties. To start with, a nonlocal stress/strain relation violates the *principle of local action* [52]: in determining the stress at a given particle, the motion outside an arbitrary neighborhood of the particle may be disregarded. This excursion out of the established framework of Continuum Mechanics has many consequences. One is the well-known difficulty to state “realistic” boundary conditions for the nonlocal variables. A similar difficulty occurred to the now almost forgotten *micropolar* models. Another consequence, less generally recognized, is that they produce solutions where the peak stresses do not occur at the domain boundaries when they should. It has been analytically proved by Simone [53] that a nonlocal models fails to predict maximum values of the stress field at the tip of a sharp crack. This is not only contrary to experience and observed behavior, but to common sense also. This, in itself, should preclude the use of this class of models from the problem of crack propagation.



A very interesting clarification on the internal workings of the nonlocal models has been recently provided by Rodriguez-Ferran et al. ([54], [55]). It is shown there that, being the differential displacement-(local)strain operator linear (for infinitesimal deformation) and being also linear the convolution operator typically used in NL models to average the strains, they can commute. In this way, a “new” NL model can be formulated where “nonlocal displacements”  $\hat{\mathbf{u}}$  are obtained by averaging of the “local displacements”  $\mathbf{u}$ . Then “nonlocal” strains are obtained in the form  $\hat{\boldsymbol{\varepsilon}} = \nabla^s \hat{\mathbf{u}}$ . Finally, a *local stress-strain relation* is used to determine the stresses. This set out is useful because it reveals that the so-called NL models really consist of a *filtering of the deformation modes*, artificially implemented to introduce a length (related to the averaging radius) into the problem. In particular, no explanation has been offered as to how to relate this length to the fracture energy of the material.

Another interesting question is which variable or variables should be non-local. Should it be the total strain, the elastic strain, the inelastic strain or some other internal variable of the model? As it is known, different combinations of these have been tried, always with different results but never with any real justification (see, for instance, Table 1 in [43], which proposes 7 different formats for an isotropic damage model).

From the practical point of view the disadvantages are also clear. First, the notion of a NL model violates the main assumption of the FEM, this being that the contribution of an individual FE to the global internal forces and stiffness can be computed from the nodal dofs of that FE. Violating this means using a data structure significantly more complex than that of a standard FEM code and, therefore, writing your own “nonlinear” code. Also, NL averaging translates in a significant increase of the number of nodes connected to a given one. The corresponding increase in the computer memory and CPU time required by the solver of equations is simply prohibitive for any real application, 3D being out of the question.

But if NL models have these serious drawbacks, why have they extended in such a way in the academic community? The reason is that they seem to be effective against the two main diseases exhibited by local models: mesh-size and mesh-bias dependence. Let us clear this out.

Nonlocal models do introduce, albeit in a very artificial manner, a length scale into the formulation. By doing so, they preclude the occurrence of any real strain localization (sharp displacement gradients) in the solution. As mesh-size dependence is a consequence of strain localizing in a band which

is only one finite element across, avoiding this cures the disease. But, unfortunately, introducing a “localization limiter” requires using FE which are 10 to 50 times smaller than the introduced length in order to show convincing resolution of the localization bands. This degree of discretization cannot be applied to real engineering applications.

Nonlocal models do not suffer from mesh-bias dependence very much for the same reason. If the occurrence of really sharp displacement gradients is hindered by the “localization limiter”, the displacement field is very smooth, and standard FE are able to reproduce it. Also, the filtering performed on the strain field acts similarly to the smoothing of non-continuous FE quantities done for post-processing purposes and used by many error estimation procedures to produce “improved” stress fields. In particular, it is easily observed that the estimation of the direction of maximum principal stress can be improved by this averaging procedure, see, for instance, [56] (note that, on the other hand, the peak stress values may be severely underestimated). It is worthwhile to remark that this beneficial averaging has always been conducted without regard to any NL concept.

## 7 Numerical examples

The formulation presented in the preceding sections is illustrated below by solving three benchmark problems. Performance of the standard continuous displacement (weak discontinuities) finite elements is tested considering standard *2 D plane-stress 3-noded linear triangular* meshes.

The examples are solved using the isotropic damage model presented in Section 3 with exponential *strain softening*, regularized according to the element size, and the global tracking algorithm presented in Section 5.

The Newton-Raphson method is used to solve the non-linear system of equations arising from the spatial and temporal discretization of the discrete weak form of the mechanical problem. In all cases 200 equal time steps are performed to complete the analyses. Convergence of a time step is attained when the ratio between the iterative and the incremental norm of the computed displacements is lower than 0.001 (0.1 %).

Calculations are performed with an enhanced version of the finite element program COMET [57], developed by the authors at the International Center for Numerical Methods in Engineering (CIMNE). Pre and post-processing is done with GiD, also developed at CIMNE [58].

## 7.1 Double edge notched specimen (DENS)

This example is selected because it corresponds to a series of tests fully documented in Nooru-Mohamed's Doctoral Thesis [59] and it has been numerically simulated in many occasions using different crack approaches ([18], [21], [60], [61]).

The specimen is square shaped and double edge notched (DENS), with dimensions  $200 \times 200 \times 50 \text{ mm}^3$ , and notch depths of 25 mm and widths of 5 mm. A schematic diagram of the geometry of the specimen and the testing arrangement is shown in Figure 6.

The experiments were designed to subject the specimen to mixed-mode tensile cracking. The DENS was placed in a special rigid loading frame to allow for the analysis of various loading paths combining shear and tension under force and/or displacement control. The specimen to be studied here was supported at the bottom and along the right-hand side below the notch. The shear force  $P_s$  was applied through the frame along the left-hand side of the specimen above the notch and the normal force  $P$  was applied at the top. The frames were glued to the specimen. The relative normal deformation in the fracture zone  $\delta$  was measured between the points marked in the sketch,

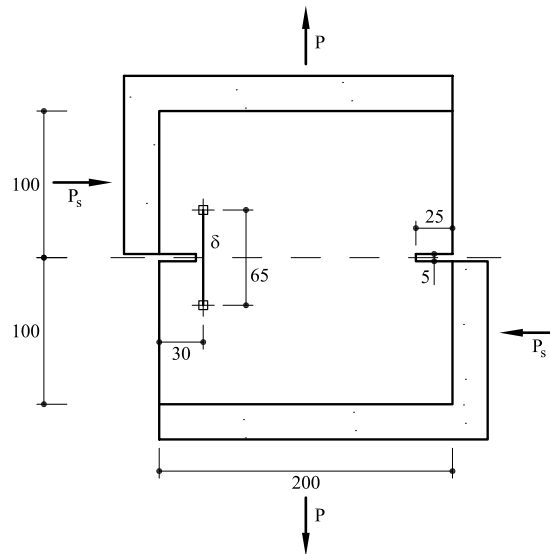


Figure 6: Geometry and load for double edge notched specimen (DENS)

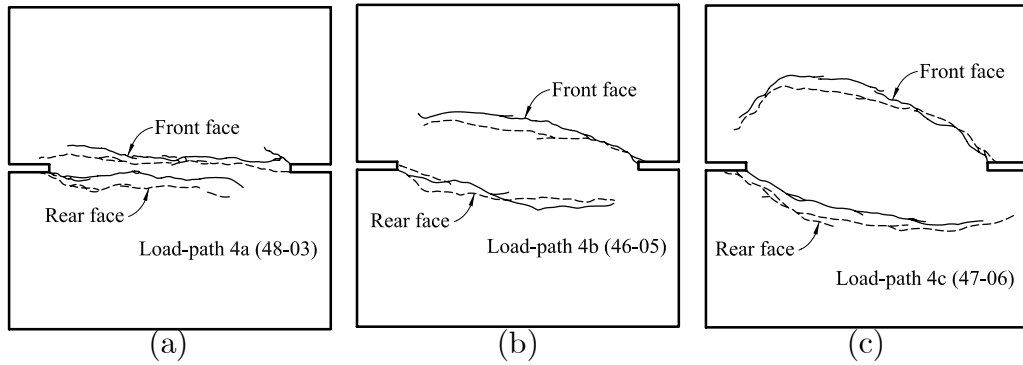


Figure 7: Experimentally obtained crack patterns for double edge notched specimens

65 mm apart and 30 mm from the left-hand side boundary.

Three different load-paths are investigated here, 4a 48-03, 4b 46-05 and 4c 47-06. They are characterized by different values of the firstly applied shear force  $P_s$  (while  $P = 0$ ): 5 kN for DENS-4a, 10 kN for DENS-4b and  $P_s^{\max} = 27.5$  kN for DENS-4c. The experiment continues by keeping the applied shear force  $P_s$  constant, while progressively increasing the axial vertical displacement. The corresponding normal reaction  $P$  is measured throughout the experiment.

Figure 7 shows the crack patterns obtained in the experiments. It should be observed that, although very interesting, these experimental results cannot be accepted unquestionably. First, the difference in cracking between the front and the rear faces indicates that the specimens were not really tested under pure membrane action, some bending may have spuriously happened. Furthermore, the cracks at the top and bottom of the specimens do not show the symmetry that would be expected from the intended boundary conditions. This may be due to a number of reasons dealing with the set up of the fixings. Anyhow, they are affecting the strain/stress field in at least one half of the specimens significantly. Other comment is that it was reported that the frame and the specimens, although being glued, suffered separation in some cases, particularly at the top-right and bottom-left corners, where some spurious cracking was observed in some specimens. Also, it is worth to mention that all the numerical simulations referred to these tests tend to evaluate peak values for the normal forces  $P$  which are overestimated when compared to the experimental values. This may be due to the mentioned de-

iciencies in the experimental set up. Finally, the specimens were of different ages in the moment of their testing. All this means that the confidence on the experimental results must be critically evaluated.

The computational domain is discretized in two different unstructured meshes of *2D plane-stress 3-noded linear triangular elements* with average mesh sizes of  $h_e = 5$  mm (2,125 nodes) and  $h_e = 2.5$  mm (8,391 nodes), not shown. Although this may seem a very refined degree of discretization, it must be observed that the difference in the global elastic stiffness under the shear forces is 7 % between the “coarse” and “fine” meshes, the latter being obviously smaller. This is because of the presence of the two notches, which render the nearby areas nearly singular. Regarding the computational boundary conditions, they have been defined exactly symmetrical, with the central node of the mesh being fixed in the horizontal and vertical dofs.

For each of the load-paths, four different analyses have been performed: (a.1) coarse mesh with tracking, (a.2) coarse mesh without tracking, (b.1) fine mesh with tracking and (b.2) fine mesh without tracking. The pre-processor used tends to introduce patches of equilateral triangles with predominant directions at  $-60^\circ$ ,  $0^\circ$  and  $+60^\circ$  with the horizontal axis, particularly for the finer mesh. The results obtained are discussed in the following.

## 7.2 Load path 4a

For load-path 4a (specimen 48-03) the loading is applied in two stages: first, a shear force  $P_s = 5$  kN is applied, while keeping the normal force  $P = 0$ ; later, the experiment continues by keeping the applied shear force  $P_s$  constant, while progressively increasing the axial vertical displacement  $\Delta$ .

The following material properties are assumed for this case: Young’s modulus  $E = 30$  MPa, Poisson’s ratio  $\nu = 0.2$ , tensile strength  $\sigma_o = 2.8$  KPa and mode I fracture energy  $G_f = 90$  J/m<sup>2</sup>.

As commented, four separate analyses are performed using th two meshes. The computed deformed shapes of the specimen are shown in Figures 8a.1 and 8b.1, for the coarse and fine meshes, respectively (imposed total vertical displacement  $\Delta = 0.2$  mm, with a displacement amplification factor of 100). The different element sizes in the meshes can be appreciated in these figures. As shown, the computed cracks in the two analyses where tracking was performed (top figures) follow very closely the same path, starting at the tip of the notches and tilting slightly due to the orientation of the strain field. No spurious mesh bias is observed in any of these analysis.

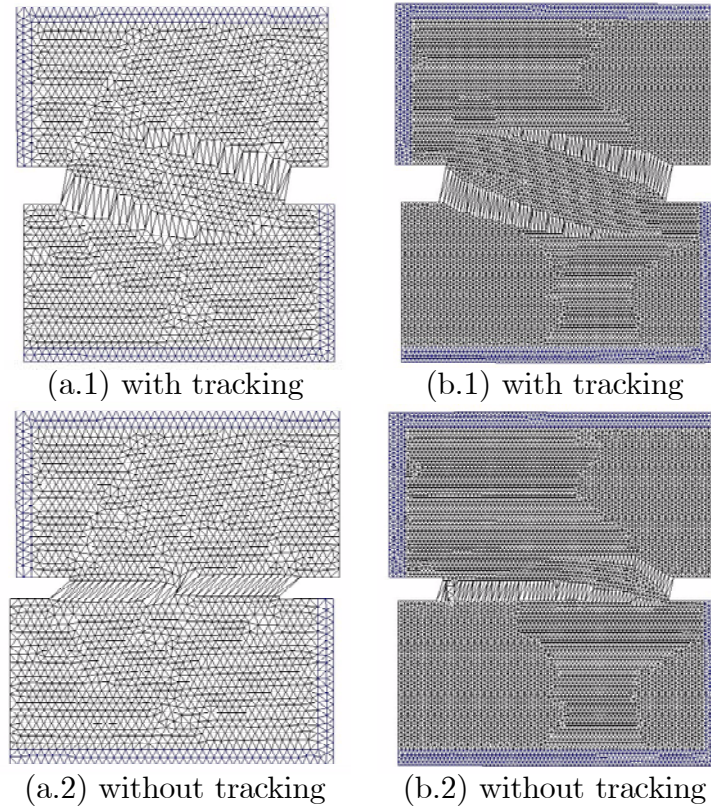


Figure 8: Deformed geometries ( $\times 100$ ) on the two meshes with and without tracking for double edge notched specimen - load path 4a

If no tracking strategy is used, see Figures 8a.2 and 8b.2, the cracks initiate correctly, but they turn horizontally almost immediately to run along with the respective mesh alignment and too close to the horizontal axis.

Figure 9 shows load vs imposed vertical displacement curves obtained with the two different meshes, and using tracking. In this example the loading branch curves slowly as the cracks progress, turning into the softening branch once the failure mechanism is fully developed. Load does not vanish completely because only damage due to tensile effective stresses is considered, and the state of stresses near the opposite notch is mostly compressive.

Note that the overall global response is very similar upon mesh refinement, although the effect of the different spatial discretizations can be observed even in the global elastic stiffness of the specimen. This shows that solving problems involving singular stress points requires a high level of resolution.

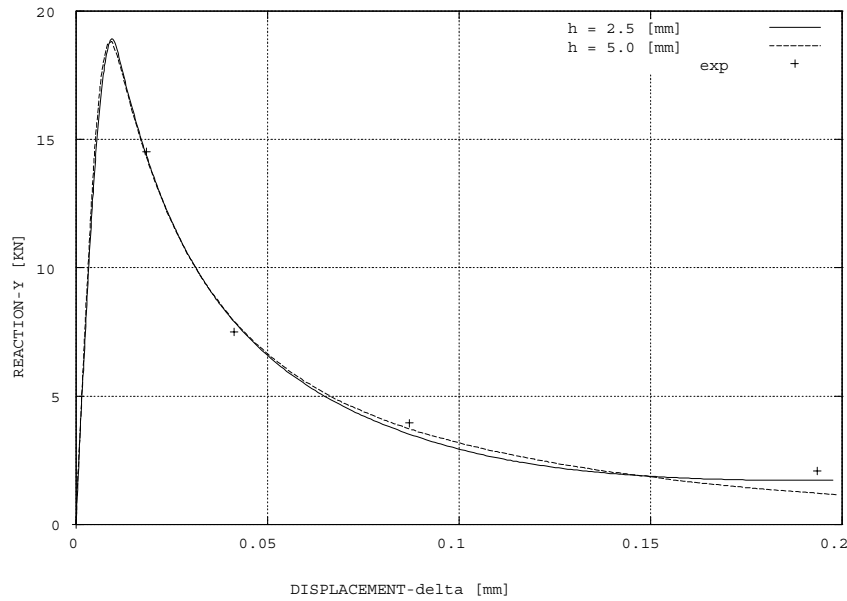


Figure 9: Load *versus* displacement for double edge notched specimen - load path 4a. Comparison between different mesh sizes

No spurious brittleness is observed when the size of the elements in the mesh is reduced.

Figure 10 shows the results obtained using the proposed formulation on the fine mesh. The three columns represent, respectively, the evolution, at three different time steps of the analysis, of: (a) the contours of total displacements, (b) the contours of the damage index and (c) the maximum principal strain vectors. The progressive concentration of the displacement gradients (strains) in the elements along the crack paths is evident in the three columns. The bottom figures show how, when the failure mechanism is fully developed, all the deformation concentrates in the formed cracks, while the elements outside these bands are mostly undeformed. Note that the resolution of the cracks is optimal for the mesh used. Observe in the left bottom plot how, once both cracks are formed, the central part of the specimen rotates almost as a rigid body around the center of the specimen. For the coarser mesh, similar results are obtained, although the strain localization is smeared across a row of larger elements (see Fig. 8).

In the third column, it can be observed that, although this experiment has

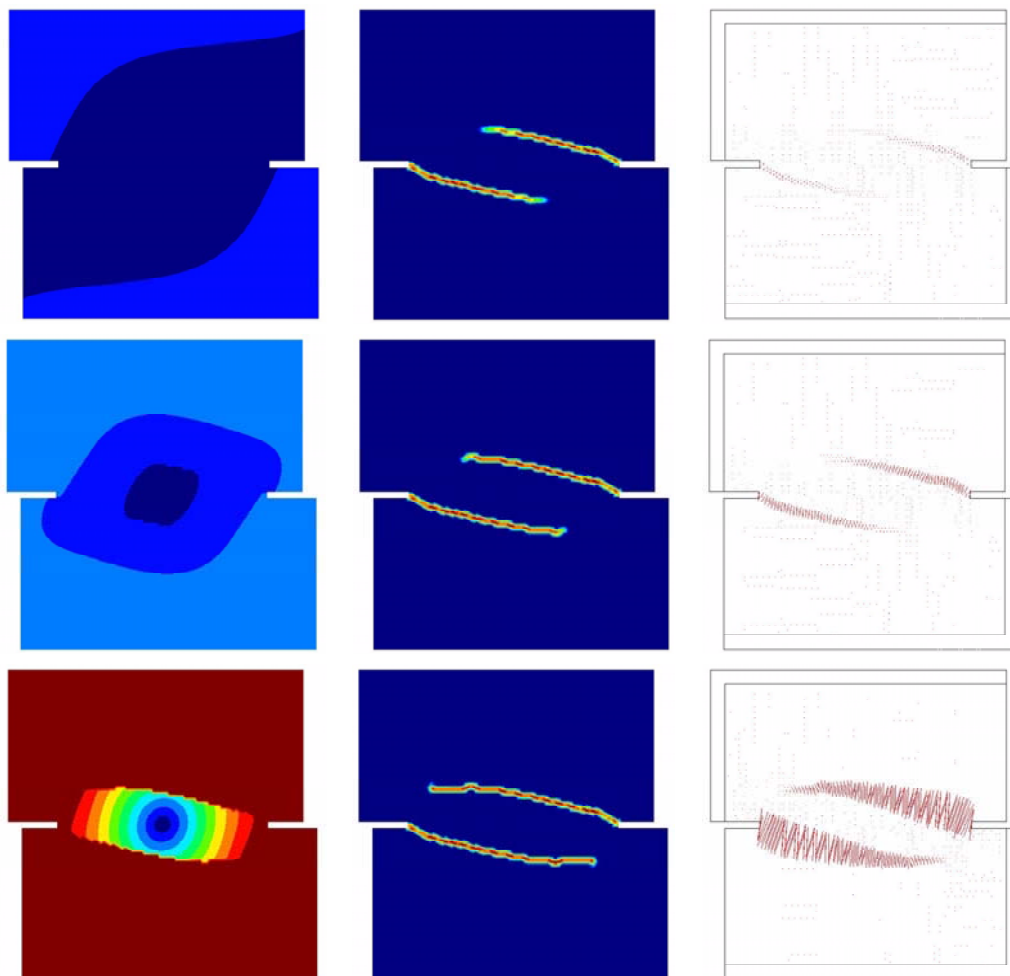


Figure 10: Results for double edge notched specimen (load path 4a) using the proposed formulation. Evolution of: (a) displacement, (b) damage, (c) vectors of max. principal strain

been devised as a mixed-mode cracking test, and the cracks indeed initiate at an angle from the notches, the failure mechanism is mainly in pure mode I, as the computed maximum tensile principal strain vectors (as the related vectors of maximum tensile principal effective stress) are mostly orthogonal to the crack path. Note also that the correct failure mechanism has been predicted although the directions of some of the computed maximum principal strain vectors are clearly dependent on the mesh bias, as they are not orthogonal



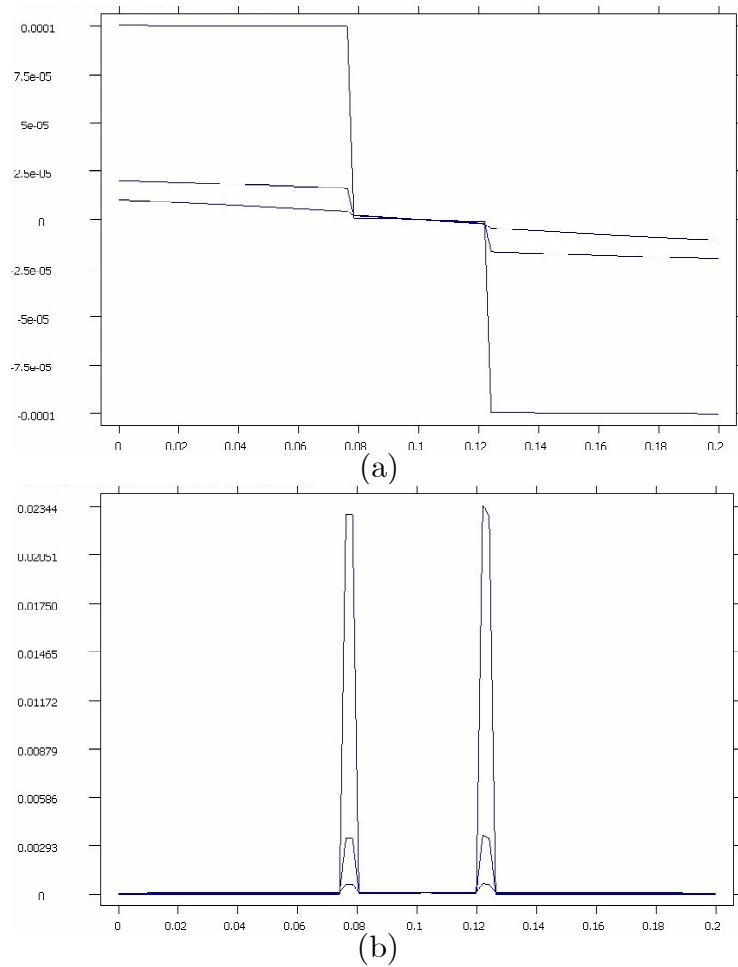


Figure 11: Evolution of the profiles along the central vertical axis of: (a) vertical displacement and (b) maximum principal strain for double edge notched specimen (load path 4a)

to the crack path everywhere.

Finally, Figures 11a and 11b show the evolution, at three different time steps of the analysis, of: (a) the vertical displacement and (b) the maximum principal strain, along a vertical line along the centre of the specimen which crosses both cracks. In these, it can be observed how the initially smooth gradient of displacements progressively localizes into two very sharp (but weak) jumps across one single element. Also, the strain profile progressively localizes with very sharp resolution of the two (weak) discontinuities formed.

It is here shown that, in practice, there exists little difference between a highly resolved weak discontinuity and a strong discontinuity.

### 7.3 Load path 4b

For load-path 4b (specimen 46-05) the loading is also applied in two stages: first, a shear force  $P_s = 10$  kN is applied, while keeping the normal force  $P = 0$ ; later, the experiment continues by keeping the applied shear force  $P_s$  constant, while progressively increasing the axial vertical displacement  $\Delta$ .

The following material properties are assumed for this case: Young's modulus  $E = 30$  MPa, Poisson's ratio  $\nu = 0.2$ , tensile strength  $\sigma_o = 2.2$  KPa and mode I fracture energy  $G_f = 80$  J/m<sup>2</sup>.

Again, four separate analyses are performed using the two different meshes.

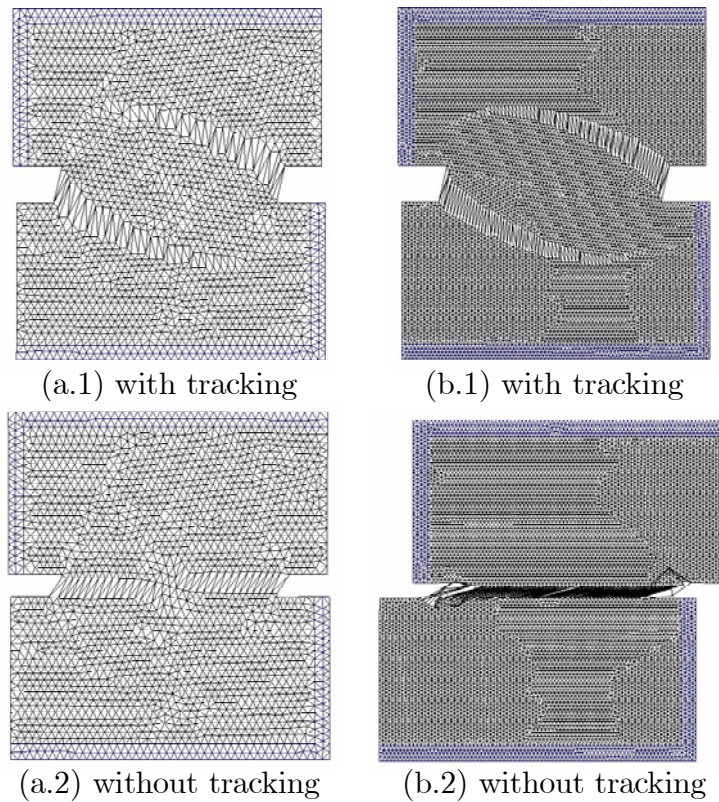


Figure 12: Deformed geometries (x 100) on the two meshes with and without tracking for double edge notched specimen (load path 4b)

The computed deformed shapes of the specimen are shown in Figures 12a.1 and 12b.1, for the coarse and fine meshes, respectively (imposed total vertical displacement  $\Delta = 0.2$  mm, with a displacement amplification factor of 100). As shown, the computed cracks in the two analyses where tracking was performed (top figures) follow very closely the same path, starting at the tip of the notches and tilting markedly due to the orientation of the strain field. No spurious mesh bias is observed in any of these analysis. The elevation that the top crack reaches above the horizontal axis matches almost exactly that observed in the experiment (see Fig. 7b).

If no tracking strategy is used, see Figures 12a.2 and 12b.2, the cracks are practically horizontal, running along with the mesh alignment and practically coinciding with the horizontal axis. The analysis on the fine mesh fails along this axis at a much earlier stage than expected.

Figure 13 shows load vs imposed vertical displacement curves obtained with the two different meshes, and using tracking. In this example the loading branch curves more slowly as the cracks progress, turning into the softening

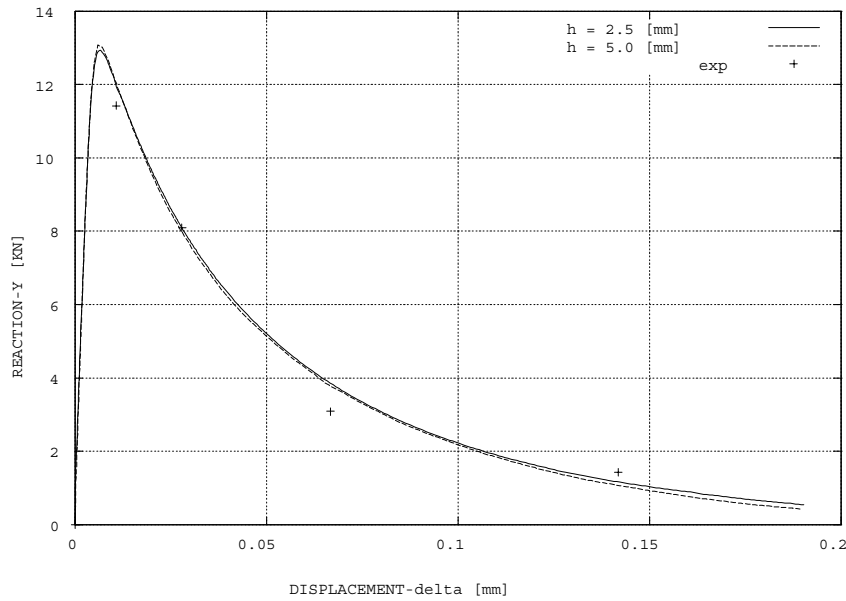


Figure 13: Load versus displacement for double edge notched specimen - load path 4b. Comparison between different mesh sizes

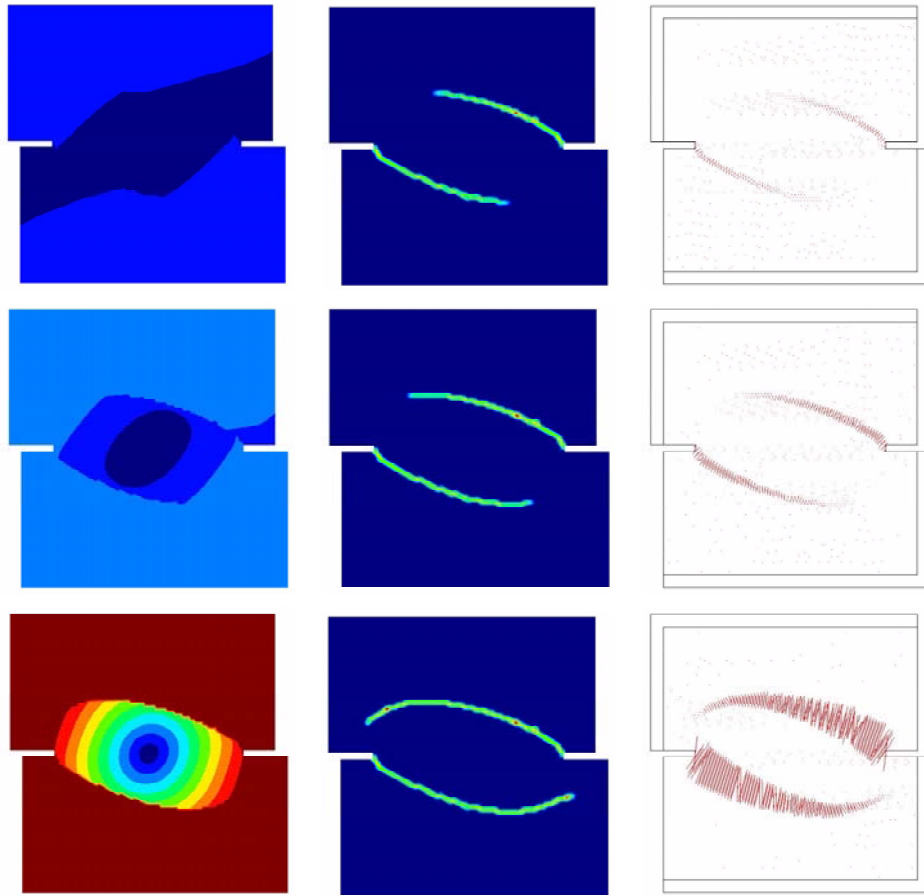


Figure 14: Results for double edge notched specimen (load path 4b) using the proposed formulation. Evolution of: (a) displacement, (b) damage, (c) vectors of max. principal strain

branch once the failure mechanism is fully developed. Load almost vanishes completely at the end of the analyses.

As in the previous example, the overall global response is very similar upon mesh refinement, and no spurious brittleness is observed when the size of the elements in the mesh is reduced.

Figure 14 shows the results obtained using the proposed formulation on the fine mesh. The three columns represent, respectively, the evolution, at three different time steps of the analysis, of: (a) the contours of total displacement, (b) the contours of the damage index and (c) the maximum

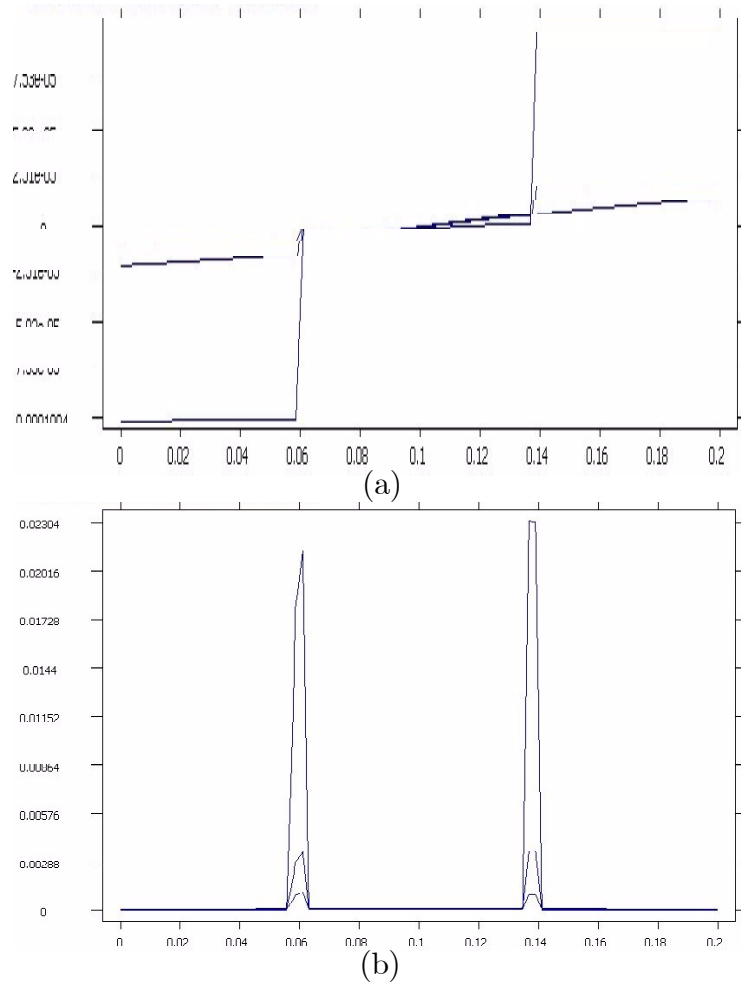


Figure 15: Evolution of the profiles along the central vertical axis of: (a) vertical displacement and (b) maximum principal strain for double edge notched specimen (load path 4b)

principal strain vectors. The progressive concentration of the displacement gradients (strains) in the elements along the crack paths is evident in the three columns. The bottom figures show how, when the failure mechanism is fully developed, all the deformation concentrates in the formed cracks, while the elements outside these bands are mostly undeformed. The resolution of the cracks is optimal for the mesh used. For the coarser mesh, similar results are obtained, although the strain localization is smeared across a row of larger elements (see Fig. 12).

In the third column, it can be observed again that the dominant mechanism for the progression of the crack is an almost pure tensile mode I, despite the shearing stress/strain fields applied. Note that the correct crack path is predicted although the directions of the computed maximum principal strain vectors are clearly dependent on the mesh bias, as they are not necessarily orthogonal to the crack path.

Finally, Figures 15a and 15b show the evolution, at three different time steps of the analysis, of: (a) the vertical displacements, (b) the maximum principal strain, along a vertical line along the centre of the specimen which crosses both cracks. Again, it can be observed how it is difficult to maintain that there are practical differences between such highly resolved weak discontinuities and a strong ones.

## 7.4 Load path 4c

For load-path 4c (specimen 47-06) the loading is also in two stages: first, the maximum shear force that the specimen can sustain,  $P_s^{\max} = 27.5$  kN, is applied, while keeping the normal force  $P = 0$ ; later, the experiment continues by keeping the applied shear force  $P_s^{\max}$  constant, while progressively increasing the axial vertical displacement  $\Delta$ .

The following material properties are assumed for this case: Young's modulus  $E = 30$  MPa, Poisson's ratio  $\nu = 0.2$ , tensile strength  $\sigma_o = 2.2$  KPa and mode I fracture energy  $G_f = 80$  J/m<sup>2</sup>.

As commented, four separate analyses are performed using the coarse and fine meshes. In the FE analyses, the maximum shear force sustained by the coarse mesh was  $P_s^{\max} = 27.5$  kN, but the fine mesh sustained a slightly higher shear force of  $P_s^{\max} = 28.6$  kN (6 % higher) to reach the same state of crack propagation. This is due to the 7 % difference in the global stiffness of the two meshes. This explains the differences observed in the corresponding responses during the later stage of axial straining.

The computed deformed shapes of the specimen are shown in Figures 16a.1 and 16b.1, for the coarse and fine meshes, respectively (imposed total vertical displacement  $\Delta = 0.2$  mm, with a displacement amplification factor of 100). As shown, the computed cracks in the two analyses where tracking was performed (top figures) follow very closely the same path, starting at the tip of the notches and progressively curving inwards due to the reorientation of the strain field. Agreement with the experimental pattern (see Fig. 7c) is remarkable. No spurious mesh bias is observed in any of these analysis.

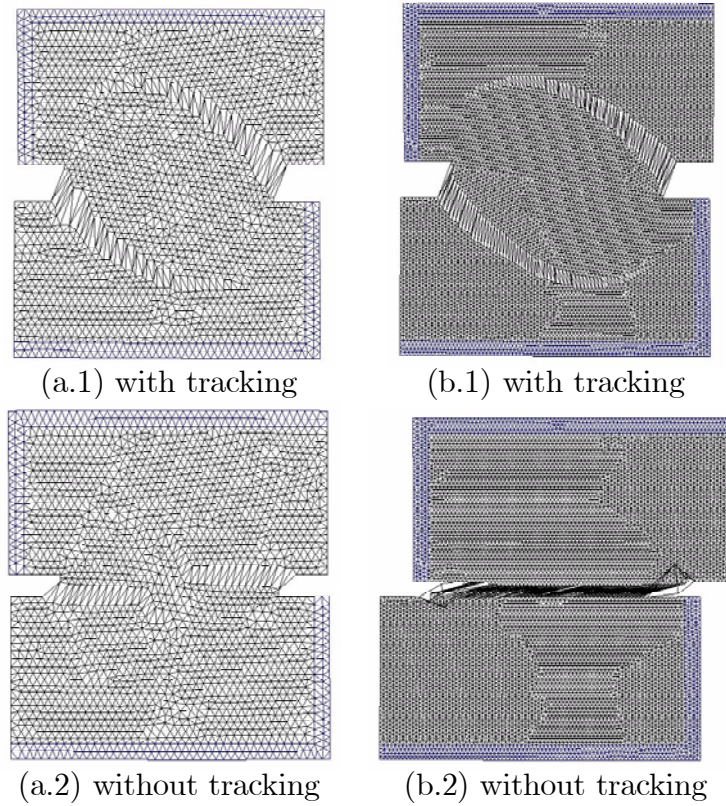


Figure 16: Deformed geometries (x 100) on the two meshes with and without tracking for double edge notched specimen (load path 4c)

If no tracking strategy is used, see Figures 16a.2 and 16b.2, the cracks form almost horizontally, in a totally unrealistic manner. As in the previous example, the analysis performed with the fine mesh fails prematurely.

Figure 17 shows load vs imposed vertical displacement curves obtained with the two different meshes, and using tracking. This graph is surprising, as it shows that the axial force  $P$  turns rapidly to be negative, even if the applied axial displacement is positive, corresponding to pulling apart the fixing frames. Only reference [61] reports success in modelling this curious result, while reference [60] clearly states that the model used there cannot reproduce this compressive state.

Note that the value of the normal forces  $P$  involved in this case is much lower than the shear forces  $P_s^{\max}$ . This explains the relative difference in the results obtained with the two meshes.

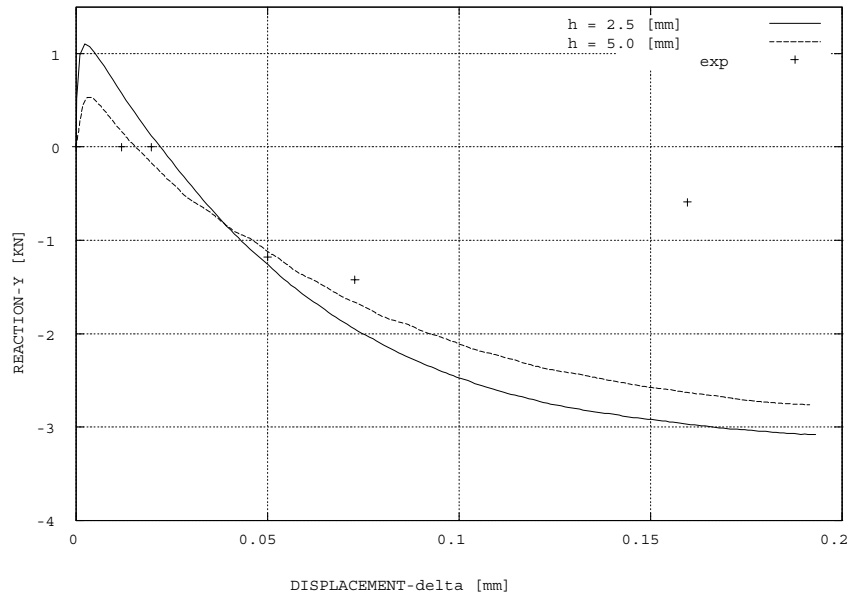


Figure 17: Load versus displacement for double edge notched specimen - load path 4c. Comparison between different mesh sizes

Figure 18 shows the results obtained using the proposed formulation on the fine mesh. As in the previous cases, the three columns represent, respectively, the evolution, at three different time steps of the analysis, of: (a) the contours of total displacement, (b) the contours of the damage index and (c) the maximum principal strain vectors. The progressive concentration of the displacement gradients (strains) in the elements along the crack paths is evident in the three columns and it is very clear in the bottom figures. For the coarser mesh, similar results are obtained, although the strain localization is smeared across a row of larger elements (see Fig. 16).

Finally, Figures 19a and 19b show the evolution, at three different time steps of the analysis, of: (a) the vertical displacements, (b) the maximum principal strain, along a vertical line along the centre of the specimen which crosses both cracks. Comments are similar to those expressed for the previous load cases.



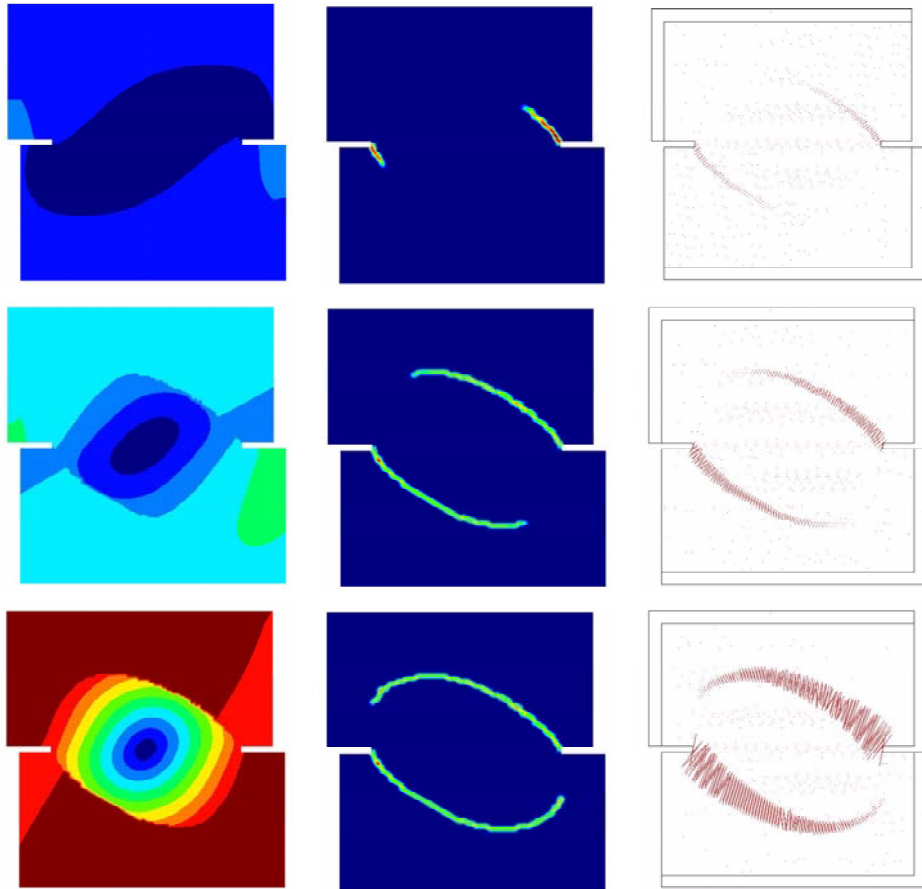


Figure 18: Results for double edge notched specimen (load path 4c) using the proposed formulation. Evolution of: (a) displacement, (b) damage, (c) vectors of max. principal strain

## 8 Conclusions

This paper shows the application of *standard finite elements* with continuous displacement fields, such as linear triangles, to the solution of problems involving the propagation of tensile cracks using the classical smeared crack approach, that is, via a *local* isotropic continuum damage model with properly regularized strain softening.

A mesh objective formulation of the problem is obtained, which translates in the achievement of three crucial goals:

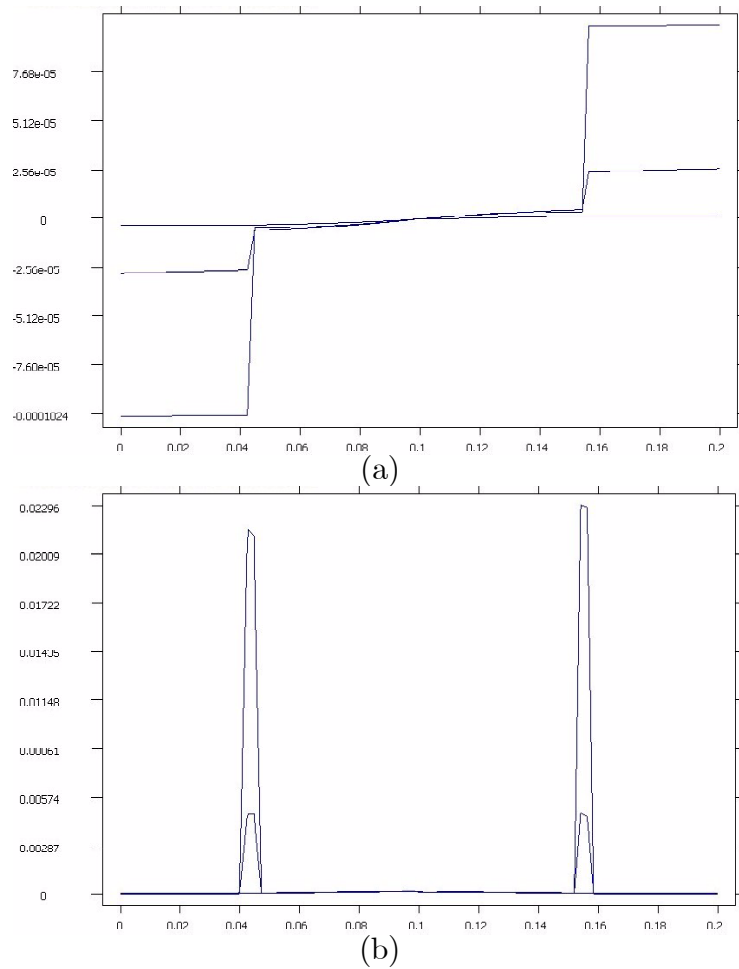


Figure 19: Evolution of the profiles along the central vertical axis of: (a) vertical displacement and (b) maximum principal strain for double edge notched specimen (load path 4c)

1. the solution of the corresponding boundary value problem exists and it is unique,
2. the position and orientation of the localization paths (cracks) is independent of the directional bias of the finite element mesh, and
3. the global post-peak load-deflection curves are independent of the size of the elements in the localization path (crack).

The accomplishment of these objectives is attained by considering the

determination of the direction of propagation of the strain localization band as a separate problem, coupled to that of solving the equation of internal equilibrium. The necessity of doing this stems from previous experience with the discrete crack approach, both in the *fracture* and *continuum* mechanics frameworks, but it is also deduced from the stability analysis of the weak forms of the associated mechanical problem, both in continuum and discrete formats.

The smeared formulation is compared to the discrete approach resulting from applying the so-called strong discontinuity approach. It is shown that both approaches are similar in many ways. Non local constitutive models are also discussed, concluding that, albeit their current trendiness, they are not suitable for the problem of crack propagation.

Numerical examples show, on one hand, the tremendous advantage of using a crack propagation algorithm to predict correct failure mechanisms with localized patterns of tensile deformation, virtually free from any dependence of the mesh directional bias; on the other, these techniques are shown to produce results which exhibit the correct amount of dissipated energy during the localization (fracture) process, directly related to the fracture energy of the material, yielding a correct global response in the softening regime. Finally, computed solutions show that, as expected, the weak discontinuity concept converges upon mesh refinement to the strong discontinuity approach.

The proposed smeared approach is shown to be convergent upon mesh refinement, virtually free of the spurious size and bias mesh dependence usually found when directly applying the smeared crack concept to strain localization problems. The derived method yields a robust scheme, suitable for engineering applications in 2D and 3D.

## Acknowledgments

The authors gratefully acknowledge the invaluable help of our colleague Prof. R. Codina, expressed in the form of so many suggestions and fruitful discussions.

## References

- [1] Galilei, G. (1638). Discorsi e dimonstrazioni matematiche intorno a due

nuove scienze. English translation: Two new sciences, The Macmillan Company (1933), New York.

- [2] Griffith, A.A. (1921). The phenomenon of rupture and flow of solids. *Phil. Trans. Roy. Soc. (London)*, 22, 163-198.
- [3] Barenblatt, G.I. (1959). On equilibrium cracks formed during brittle fracture. *Prikl. Mat. Mech.*, 23, 3, 622-636 .
- [4] Dugdale, D.S. (1960). Yielding of steel seets containing slits. *J. of the Mechanics and Physics of Solids*, 8, 100–104.
- [5] Cervera, M., Chiumenti and Agelet de Saracibar, C. 2003. Softening, localization and stabilization: capture of discontinuous solutions in  $J_2$  plasticity. *Int. J. for Num. and Anal. Meth. in Geomechanics*, 28, 373-393.
- [6] Cervera, M., Chiumenti and Agelet de Saracibar, C. 2003. Shear band localization via local  $J_2$  continuum damage mechanics. *Comp. Meth. in Appl. Mech. and Eng.*, 193, 849-880.
- [7] Clough, R.W. (1962). The stress distribution of Norfolk Dam. *Structures and Materials Research, Department of Civil Engineering Series 100*, 19, University of California, Berkeley, California, USA.
- [8] Ngo, D. and Scordelis, A.C. (1967). Finite element analysis of reinforced concrete beams. *ACI Journal*, 64(14), 152-163.
- [9] Nilson, A.H. (1968). Nonlinear Analysis of Reinforced Concrete by the Finite Element Method. *ACI Journal*, 65(9), 757-776.
- [10] Tong, P. and Pian, T.H.H. (1973). On the convergence of the finite element method for problems with singularity. *Int. J. Solids struct.*, 9, 313-321.
- [11] Owen, D.R.J. and Fawkes, A.J. (1983). *Engineering Fracture Mechanics*, Pineridge Press, Swansea.
- [12] Belytschko, T. and Black, T. (1999). Elastic crack growth in finite elements with minimal remeshing. *Comp. Meth. in Appl. Mech. and Eng.*, 45(5), 601-620.

- [13] Möes, N., Dolbow, J. and Belytschko, T. (1999). A finite element method for crack growth without remeshing. *Int. J. Num. Meths. in Engng.*, 46, 131-150.
- [14] Sukumar, N., Möes, N., Moran, B. and Belytschko, T. (2000). Extended finite element method for three-dimensional crack modelling. *Int. J. Num. Meths. in Engng.*, 48, 1549-1570.
- [15] Simo, J.C., Oliver, J. and Armero, F. (1993). An analysis of strong discontinuities induced by strain-softening in rate-independent inelastic solids. *Computational Mechanics*, 12, 49-61.
- [16] Oliver, J. (1995). Continuum modeling of strong discontinuities in solid mechanics using damage models. *Computational Mechanics*, 17, 277-296.
- [17] Oliver, J., Cervera, M. and Manzoli, O. (1999). Strong discontinuities and continuum plasticity models: the strong discontinuity approach. *Int. J. of Plasticity*, 15, 319-351.
- [18] Oliver, J., Huespe, A.E. Samaniego, E. and Chaves, W.V.. (2004). Continuum approach to the numerical simulation of material failure in concrete. *Int. J. for Num. and Anal. Meth. in Geomechanics.*, 28, 609-632.
- [19] Oliver, J. and Huespe, A.E. (2004). Theoretical and computational issues in modelling material failure in strong discontinuity scenarios. *Comp. Meth. in Appl. Mech. and Eng.*, 193, 2987-3014.
- [20] Oliver, J. and Huespe, A.E. (2004). Continuum approach to material failure in strong discontinuity settings. *Comp. Meth. in Appl. Mech. and Eng.*, 193, 3195-3220.
- [21] Feist, C., Kerber, W., Lehar, H. and Hofstetter, G. (2004). A comparative study of numerical models for concrete cracking. *Proceedings of European Congress on Computational Methods in Applied Sciences and Engineering, ECCOMAS 2004*, Neittaanmäki, P., Rossi, T., Korotov, S., Oñate, E., Periaux, J. and Knörzer, D. (eds.), Jyväskylä, Finland.
- [22] Rashid, Y. (1968). Analysis of prestressed concrete pressure vessels. *Nuclear Engineering and Design*, 7, 334-344.

- [23] Hillerborg, A., Modeer, M., and Peterson, P.E. (1976). Analysis of crack formation and crack growth in concrete by means of F. M. and finite elements. *Cement and Concrete Research*, 6.
- [24] Bazant, Z.P. and Oh, B.H. (1983). Crack band theory for fracture of concrete. *Material and Structures*, 16, 155-177.
- [25] de Borst, R. (2002). Fracture in quasi-brittle materials: a review of continuum damage-based approaches. *Engineering Fracture Mechanics*, 69, 95-112.
- [26] Cervera, M., Oliver, J., and Faria, R. (1995). Seismic evaluation of concrete dams via continuum damage models. *Earth. Engng. Struc. Dyn.*, 24, 1225–1245.
- [27] Cervera, M., Oliver, J., and Manzoli, O. (1996). A rate-dependent isotropic damage model for the seismic evaluation of concrete dams. *Earth. Engng. Struc. Dyn.*, 25, 987–1010.
- [28] Faria, R., Oliver, J., and Cervera, M. (1998). A strain-based plastic viscous-damage model for massive concrete structures. *Int. J. Solids and Structures*, 35(14):1533–1558.
- [29] Faria, R., Oliver, J., and Cervera, M. (1999). On isotropic scalar damage models for numerical analysis of concrete structures. *Research Publication, CIMNE, PI-170*.
- [30] Finchant, S, La Borderie, C. and Pijaudier-Cabot, G. (1999). Isotropic and anisotropic descriptions of damage in concrete structures. *Mechanics of Cohesive-Frictional Materials*, 4, 339-359.
- [31] Zienkiewicz, O.C., Pastor, M. and Huang, M. (1995). Softening, localization and adaptive remeshing: capture of discontinuous solutions. *Comp. Mech.*, 17, 98-106.
- [32] Zienkiewicz O.C., Huang, M. and Pastor, M. (1995). Localization problems in plasticity using finite elements with adaptive remeshing. *Int. J. Num. Methods in Geomechanics*, 19, 127-148.
- [33] Aifantis, E.C., 1984. On the microstructural origin of certain inelastic models. *Transactions ASME Journal of Engineering Materials Technology*, 106, 326-330.

- [34] de Borst, R. (1991). Simulation of strain localization: a reappraisal of the Cosserat continuum. *engineering computations*, 8, 317-322.
- [35] Steinmann, P. and Willam, K. (1992). Localization within the framework of micropolar elastoplasticity. In *Advances in Continuum Mechanics*. ed. V. Mannl et al. pp. 296-313. Springer Verlag, Berlin.
- Aifantis, E.C. (1984). On the microstructural origin of certain inelastic models. *Transactions ASME Journal of Engineering Materials Technology*, 106, 326-330.
- [36] Schreyer, H. and Chen, Z. (1986). One dimensional softening with localization. *Journal of Applied Mechanics, ASME*, 53, 791-797.
- [37] Vardoulakis, I. and Aifantis, E.C. (1991). A gradient flow theory of plasticity for granular materials. *Acta Mechanica*, 87, 197-217.
- [38] de Borst, R. and Mulhaus, H.B. (1992). Gradient-dependent plasticity: formulation and algorithm aspect. *Int. J. Num. Meths. in Engng.*, 35, 521-539.
- [39] Pamin, J. (1994). *Gradient-Dependent Plasticity in Numerical Simulation of Localization Phenomena*. Ph. D. Thesis, TU Delft, The Netherlands.
- [40] Peerlings, R.H.J., de Borst, R., Brekelmans, W.A. M. and Geers, M.G.D. (1998). Gradient-enhanced damage modelling of concrete failures. *Mechanics of Cohesive-Frictional Materials*, 4, 339-359.
- [41] Jirásek, M. (1998). Nonlocal models for damage and fracture: comparison of approaches. *Int. J. Solids and Structures*, 35, 4133-4145.
- [42] de Borst, R. (2001). Some recent issues in computational failure mechanics. *Int. J. Num. Meths. in Engng.*, 52, 63-95.
- [43] Bazant, Z. and Jirásek, M. (2002). Nonlocal Integral Formulations of Plasticity and Damage: Survey of Progress. *J. of Engineering Mechanics, ASCE*, 128, 1119-1149.
- [44] Kachanov, L. M. (1958). Time of rupture process under creep conditions. *Izvestia Akademii Nauk, Old Tech Nauk*, 8, 26-31.

- [45] Lemaitre, J. and Chaboche, J. L. (1978). Aspects phénoménologiques de la rupture par endommagement. *J. Méc. Appl.*, 2, 317–365.
- [46] Lemaitre, J. and Chaboche, J.-L. (1990). *Mechanics of solid materials*. Cambridge University Press, Cambridge, U. K.
- [47] Oliver, J. (1989). A consistent characteristic length for smeared cracking models. *Int. J. Num. Meth. Engng.*, 28, 461–474.
- [48] Oliver, J. (2000). On the discrete constitutive models induced by strong discontinuity kinematics and continuum constitutive equations. *Int. J. Solids and Structures*, 37, 7207–7229.
- [49] Dumstorff, P. and Meschke, G. (2004). Investigation of crack growth criteria in the context of the extended finite element method. *Proceedings of European Congress on Computational Methods in Applied Sciences and Engineering, ECCOMAS 2004*, Neittaanmäki, P., Rossi, T., Koro-tov, S., Oñate, E., Periaux, J. and Knörzer, D. (eds.), Jyväskylä, Finland.
- [50] Mosler, J. and Meschke, G. (2004). Embedded crack vs. smeared crack models: a comparison of elementwise discontinuous crack path approaches with emphasis on mesh bias. *Comp. Meth. in Appl. Mech. and Eng.*, 193, 3351-3375.
- [51] Zienkiewicz, O.C. and Taylor, R.L. (2000). *The Finite Element Method*, Butterworth-Heinemann, Oxford.
- [52] Malvern, L.E. (1969). *Introduction to the Mechanics of a Continuum Medium*. Prentice-Hall, Englewood Cliffs, New Jersey, USA.
- [53] Simone, A.. (2003). *Continuous-Discontinuous Modelling of Failure*. Ph. D. Thesis, TU Delft, The Netherlands.
- [54] Rodriguez-Ferran, A., Morata, I. and Huerta, A. (2004). Efficient and reliable nonlocal damage models. *Comp. Meth. in Appl. Mech. and Eng.*, 193, 3431-3455.
- [55] Rodriguez-Ferran, A., Morata, I. and Huerta, A. (2004). A new damage model based on nonlocal displacements. Accepted for publication in *Int. J. for Num. and Anal. Meth. in Geomechanics*.



- [56] Grassl, P. and Jirásek, M., (2004). Fracture Mechanics of Concrete Structures, Proceedings of FraMCoS-5, Vail, Colorado, USA.
- [57] Cervera, M., Chiumenti and Agelet de Saracibar, C. (2002). COMET: COupled MEchanical and Thermal analysis. Data Input Manual, Version 5.0, Technical report IT-308, [www.cimne.upc.es](http://www.cimne.upc.es).
- [58] GiD: the personal pre and post-processor (2002). [www.gid.cimne.upc.es](http://www.gid.cimne.upc.es).
- [59] Nooru-Mohamed, M.B. (1992), Mixed mode fracture of concrete: an experimental approach. Ph. D. Thesis, TU Delft, The Netherlands.
- [60] Di Prisco, M., Ferrara, L., Meftah, F., Pamin, J., de Borst, R., Mazars, J. and Reynouard, J.M. (2000). Mixed mode fracture in plain and reinforced concrete: some results on benchmark tests. *Int. J. of Fracture*, 103, 127-148.
- [61] Pazák, B. and Jirásek, M. (2003). Adaptive simulation of quasibrittle failure: In *Computational Modelling of Concrete Structures*, Proceedings of EURO-C 2003 Conference, Bicanic, N., de Borst, R., Mang, H. and Meschke, G. (eds.), St. Johann im Pongau, Austria. A.A. Balkema Publishers.